REPUBLIC OF TURKEY

ALTINBAŞ UNIVERSITY

Institute of Graduate Studies

Electrical and Computer Engineering

DRONES SWARM FREE-SPACE OPTICAL COMMUNICATION WITH POINTING ERROR

Abdullah Jameel MAHDI AL-SAMMARRAIE

Doctor of Philosophy

Supervisor

Prof. Dr. Osman Nuri UCAN

Istanbul, 2022

DRONES SWARM FREE-SPACE OPTICAL COMMUNICATION WITH POINTING ERROR

Abdullah Jameel MAHDI AL-SAMMARRAIE

Electrical and Computer Engineering

Doctor of Philosophy

ALTINBAŞ UNIVERSITY

2022

The thesis titled (DRONES SWARM FREE SPACE OPTICAL COMMUNICATION WITH POINTING ERROR) prepared by (ABDULLAH JAMEEL MAHDI AL-SAMMARRAIE) and submitted on (17/02/2022) has been **accepted unanimously of votes** for the degree of Ph.D. in Electrical and Computer Engineering.

____

Prof. Dr. Osman Nuri UCAN

Supervisor

Thesis Defense Committee Members:

Prof. Dr. Osman Nuri UCAN	Faculty of Engineering and Architecture Altinbas University	_______________
Prof. Dr. Oguz BAYAT	Faculty of Engineering and Architecture Altinbas University	______________
Asst. Prof. Dr. Sefer KURNAZ	Faculty of Engineering and Architecture Altinbas University	____________
Asst. Prof. Serdar KARGIN	Faculty of Electronic and Architecture Beykent University	_____________
Assoc. Prof. Dr. Wamidh JALIL	Faculty of Electrical Engineering Southern Technical University	_____________

I hereby declare that this thesis meets all format and submission requirements of a Ph.D. thesis.

Submission date of the thesis to the Graduate Education Institute: ___/___/___.

I hereby declare that all information/data presented in this graduation project has been obtained in full accordance with academic rules and ethical conduct. I also declare all unoriginal materials and conclusions have been cited in the text and all references mentioned in the Reference List have been cited in the text, and vice versa as required by the abovementioned rules and conduct.

Abdullah Jameel MAHDI AL-SAMMARRIAE

Signature

DEDICATION

This dissertation I dedicate to my family members for their sacrifice and patience for the shortcomings that I showed during the four years of the program. As well as everything I can do, I would be honored to dedicate this dissertation to my parents. The two-person gave me the tools and values necessary to be where I am standing today. My appreciation goes to Prof. Dr. Osman Nuri Ucan and the Assoc. Prof. Dr. Wahmidh Jalil Mezhar for their guidance in preparing the final document. I do not forget the encouragement and support of my brothers and sisters to ease the troubles and difficulties I faced in my studies. Finally, I dedicated this work to my lovely daughter Sama.

ACKNOWLEDGEMENTS

I would like to express my gratitude towards Assoc. Prof. Dr. Wamidh Jalil Mezhar for guiding me throughout the dissertation. I also express my kind gratitude to our principal Prof. Dr. Oguz Bayat for allowing me to conduct the "Drones Swarm Free Space Optical Communication With Pointing Error" thesis. The mentioned project was done under the supervision of the Prof. Dr. Osman Nuri Ucan. I thank all participants for their positive support and guidance. I feel thankful to the college staff for giving me such a big opportunity.

ABSTRACT

DRONES SWARM FREE SPACE OPTICAL COMMUNICATION WITH POINTING ERROR

Al-sammarraie, Abdullah Jameel Mahdi

Ph.D., Electrical and Computer Engineering, Altınbaş University,

Supervisor: Prof. Dr. Osman Nuri Ucan

Date: February/2022

Pages: (94)

Drones are one of the Unmanned Arial Vehicles (UAV) used for short-length and low-altitude applications. Applying Free Space Optical (FSO) technology is modern in drone communication systems. The FSO technology has significant features such as high security due to narrow beamwidth, insusceptible to interferences, free license, landline connection is not appropriate, etc.

The proposed system took the V-shape configuration and simulated it using MATLAB 2020. The V-shape configuration is one topology of networking topologies used in communication systems. The system has three subsystems: two Single-Input Single-Output (SISO) topologies and one Multiple-Input single-output (MISO) topology, connected by an optical beam and flying in weak atmospheric turbulence. The optical beam modulates using the PPM technique and faces many obstacles that affect the system's performance, such as the attenuation and turbulence of the atmospheric channel and misalignment.

The obstacles represented by the channel gain H consist of three factors: the pointing error factor H_P, the atmospheric attenuation H_a, and the atmospheric turbulence H_f. H_p is a significant factor that may be happening in the transmitter, receiver, or optical beam.

The related parameters to H_p are the pointing error angle θ_r, the link distance Z, and the beamwidth w_z. The pointing error angle θ_r must be $< 10^{-4}$ rad for long distances (inter-satellite application). The goal of this dissertation is to measure the allowable range of the pointing error angles θ_r that is $> 10^{-4}$ rad at specific link distance Z where the system gets high performance, and determine the link distance Z where the system failed at a specific pointing error angle θ_r.

The results showed that high system performance happens at SNR ≥ 10 dB. For pointing error angle θ_r=10^{-2}rad, the values of the applicable link distances Z are nearly 10% of the link distances Z values for θ_r=10^{-3} rad. The same percent when increasing the pointing error angle θ_r to 10^{-1} rad. Also, the results showed that the best performance was at Z$\leq$8500 m. Therefore, the system's highest altitude h system can reach $\leq$ 8500 m, depending on the drone's characteristics. Each subsystem can be considered an independent system and used in another configuration.

Keywords: Unmanned Aerial Vehicles, Free Space Optical, Radio Frequency, Single Input-Single Output, Multiple Inputs–Single Output, Pointing Error, Pointing Error Angle.

TABLE OF CONTENTS

Page

LIST OF TABLES

Page

LIST OF FIGURES

Page

LIST OF ABBREVIATIONS

UAV	:	Unmanned Arial Vehicle
FSO	:	Free Space Optical
Gb/s	:	Giga bit/second
Mb/s	:	Miga bit/second
RF	:	Radio Frequency
SISO	:	Single Input-Single Output
MISO	:	Multiple Input-Single Output
BS	:	Base station
PAT	:	Pointing-Acquistion, and Tracking
FOV	:	Field of View
WDM	:	Wavelength Division Multiplexing
LALE	:	Low Altitude Long Endurance
MALE	:	Medium Altitude Long Endurance
UAS	:	Unmanned Arial System
HAP	:	High Altitude Platform
LAP	:	Low Altitude Platform
A2A	:	Air to Air
A2G	:	Air to Ground
ICAO	:	International Civil Aviation Organization

LOS : Line-of-Sight

CNPC : Control and non-payload Communication

ITU : International Telecommunication Union

BLOS : Byond Line-of-Sight

PD : Photodetector

VCSEL : Vertical Cavity Surface Emitting Laser

VCSEL-PD: Vertical Cavity Surface Emitting Laser-Photodetector

IM/DD : Intensity Modulation/Direct Detection

BER : Bit Error Rate

BEP : Probability Error Rate

SNR : Signal-to-Noise-Ratio

AWGN : Additive White Gaussian Noise

PEP : Pairwise Error Probability

ML : Maximum Likelihood

BLOS : Byond Line Of Sight

dB : Decibel

DF : Decode and Forward

ALTM : Atmospheric Laser Turbulence Model

rad : Radian

FOR : Field of Receiver

Tx : Transmitter

Rx	:	Receiver
ABER	:	Average Bit Error Rate
WOC	:	Wireless Optical Communication
LED	:	Light Emitting Diode
LD	:	Laser Diode
MPE	:	Maximum Permissible Exposure
PPM	:	Pulse Position Modulation
SIM	:	Subcarrier Intensity Modulation
DPSK	:	Differential Pulse Shift Keying
DQPSK	:	Differential Quadrature Pulse Shift Keying
M-PPM	:	M-ary Pulse Position Modulation
IR	:	Infrared
HVB	:	Hufnagel-Valley Boundary
AoA	:	Angle-of-Arrival Fluctuation
APD	:	Avalanche Photodiode
MSLD	:	Maximum Likelihood Sequence Detection
PDF	:	Probability Distribution Function

LIST OF SYMBOLS

H : Channel gain

λ : Wavelength

θ_r : Pointing error angle

Z : Link distance

D_R : Receiver diameter

μm : Micro-meter

nm : Nano-meter

W_o : Initial beam wais

σ_I^2 : Scintillation index

I : Irradiance (intensity)

σ_x^2 : Variance of log-amplitude

C_n^2 : Refractive index structure parameter

θ_0 : Isoplantic angle

ρ_0 : Coherence length

θ : Zenith angle

σ_R^2 : Rytov variance

α : Effective number of small scale eddies

β : Effective number of large scale eddies

$\langle \beta^2 \rangle$: Angle-of-arrival

Δ: Lateral misalignment

L_p: Pointng loss

θ_{jitter}: Beam jitter angle

h: Altitude

K: Optical wave number

x: Transmitted signal

n: Additive white Gaussian noise

σ_n: Variance of the noise

R: Photodetector responsivity

H_a: Atmospheric attenuation

H_f: Atmospheric turbulence

H_p: Pointing error factor

σ: Attenuation coefficient

P_r: Received optical power

W: Beam spot radius at the receiver

r: Radial displacement

A_0: Fraction of collected power

W_{zeq}: Equivalent beam radius of the optical beam

w_z: Beam radius

a: Receiver radius

y: Received signal

1. INTRODUCTION

1.1 MOTIVATION

The drone swarm communication founded on Free Space Optical (FSO) technology is one of the Unmanned Arial Vehicle (UAV) outdoor system applications. FSO has many merits, such as high data rate, high confidence, license-free, et cetera. The success of the UAV applications has been seen in the evolution of the UAV industry. The prediction of Business Insider for that UAV sales will exceed $12 billion in 2021. Several research groups have worked on UAVs to become more powerful and efficient [1]. The outdoor or FSO is a growing technology that is cost-effective in numerous communication applications. FSO link data rates range from 1 to 2 Gb/s over distances ranging from 1 to 5 km [2]. The atmospheric's attenuation and turbulence are considered the significant challenges facing the FSO system and the line-of-sight (LOS) of an FSO link because the optical beams are narrow. Nevertheless, establishing high-reliability links appeals to several issues, such as the necessity of stringent link alignment [3]. The dissertation's system configuration depended on the previous design used in the study by Wamidh et al. [4], which took the V-shape of several drones connected optically to form the system. There were three subsystems in one system; two Single Input-Single Output (SISO) topologies, each with different parameters. One Multiple Input-Singl Output (MISO) topology has its parameters and requirements. The parameters were chosen precisely to achieve high performance. Each subsystem can be considered an independent system. The system flew in a weak turbulence regime and exposed channel gain H. The channel gain H was considered to consist of three factors. The most crucial factor is the pointing error H_p. The pointing error H_p consists of significant sub-parameters: the pointing error angle θ_r of the optical beam, the link distance Z, and the beamwidth w_z. The proposed system was simulated by MATLAB 2020. There is a limitation to using the pointing error angle θ_r [5] that had been recommended to be $< 10^{-4}$ rad for long link distances Z. The increase in the link distance Z makes the beam wider. The receiver catches a portion of the incident optical; therefore, the radial displacement r ($r \propto \theta_r$) must be as small as possible.

The dissertation is outlined in five sections, focusing on a concrete topic. In section one, the background concentrated on the advantages of using FSO over RF technology, UAV applications, the challenges facing the UAVs links such as the pointing error, the classifications and features of UAVs, UAVs' infrastructures, the objectives of this dissertation, and the literature review were the most related work. It is divided into two parts: the literature review of the pointing errors for various FSO links and a literature review for UAVs applications regarding the FSO communication systems.

Section two focused on different impairments facing the FSO link, the optical beam sources, different modulation techniques, and the detection techniques used in FSO systems. Section three described the methodology used to design and implement the proposed system using MATLAB 2020 code simulation, where the system and channel modeling and the mathematical expressions were derived. Section four presented the results and discussions depending on the mathematical expression mentioned in section three. Finally, section five was the conclusions based on the results in section four.

1.2 TECHNICAL ADVANTAGES OF FSO OVER RF-LINK

FSO technology is used as a separate communications system or a mixture of Radio Frequency (RF) technology [6]. The technology of FSO has an assortment of benefits over RF systems, such as the opponent will not detect the data during transmission. In RF technology, the opponent can monitor or jam tactical frequency and radar by using devices. In order to access information, it is also necessary to interrupt the beam directly, which is extremely difficult in FSO and easily detectable in RF systems. Furthermore, optical causes no interference with adjacent RF resources, whereas, in RF systems, the interference is highly probable. Interferences and distortions in the signal path in the opponent's jamming signals are also disadvantages of the RF link, while in FSO, there are no such drawbacks [7].

The difference between FSO and RF technologies is in the wavelength's differences, as shown in Figure 1.1, which demonstrates the optical and RF spectrum.

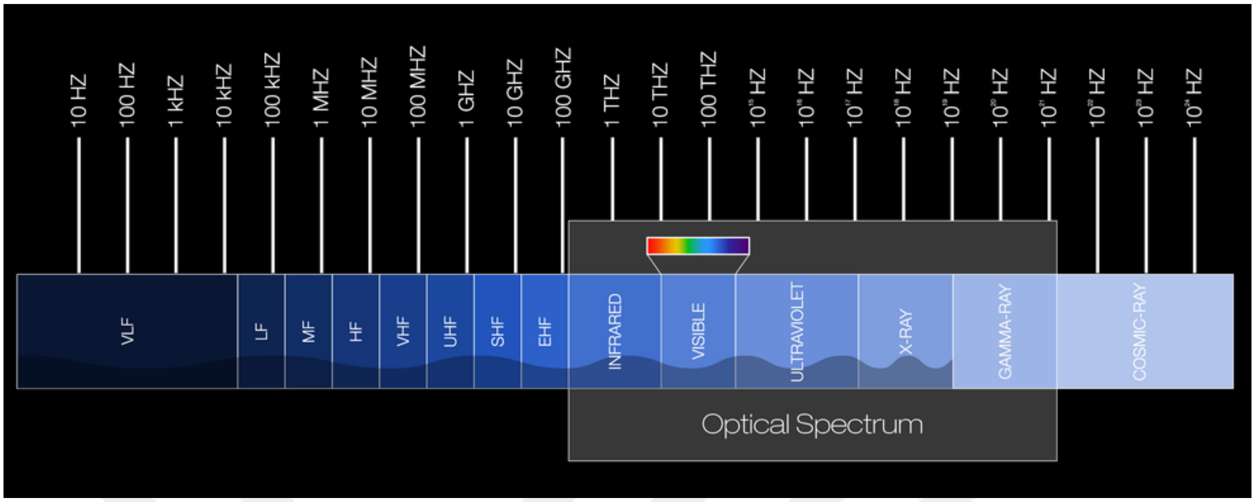

Figure 1.1: The Optical Spectrum [8].

In the FSO, when the weather conditions are clear, the character of the visibility is > 10 miles, the wavelength spectrum lies near the IR ranges between 700~1600 nm. The wavelength spectrum for the RF system range between 30 mm~3 m. So, the wavelength spectrum of the RF is higher than the FSO wavelength spectrum thousands of times. The high wavelength ratio results in several exciting contrasts between optical and RF systems, as seen below:

a. The bandwidth: high frequency increases the capacity of the link carrying information. In microwave or RF, the bandwidth used is more than twenty percent of the carrier frequency. While in FSO, if the bandwidth in use is one percent of the carrier frequency, such as the frequency ≈ 1016 Hz, the bandwidth will be 100 THz, which is practically 10^5 times that of RF.

b. Power and frame specifications are reduced**:** the beam's divergence is proportionate to λ/D_R, λ is a wavelength, and D_R is the diameter of the receiver. Therefore, the beam spreading out is slimmer than the RF beam spreading out. This characteristic increases the signal's intensity for a given power transmitted to the receiver. Figure 1.2 compares the beam divergence between the light beam and RF signals returned from Mars in the direction of the Earth. Thus, a smaller optical wavelength allows the FSO designer to develop a small antenna system than an RF to get the same gain (since the antenna gain varies inversely with the square of the operational wavelength). The optical antenna is typically 0.3 m in length, while 1.5 m for an RF antenna [9].

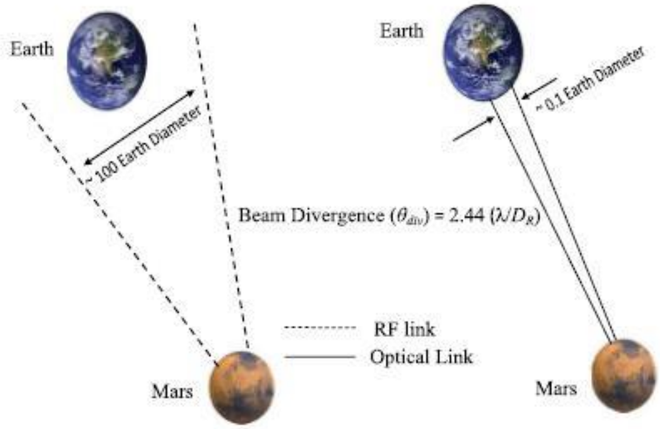

Figure 1.2: Comparison between the optical and RF beam deviation from Mars toward the Earth [9].

c. The directivity is mainly high due to the short wavelength of the optical beam, and the gain is increased [9].

d. Unlicensed spectrum: interference from neighboring carriers is a significant issue due to the spectrum congestion in RF systems. As a result, regulatory authorities would need to issue spectrum licenses. On the other hand, the optical infrastructure has been exempt from spectrum licensing; consequently, the setup and development time cost is reduced [9].

e. The beam of the FSO laser is very directional with very narrow beam separation; the spectrum analyzers and RF meters cannot detect FSO contact; consequently, high security. As a result, any form of interception is complicated. Furthermore, the FSO signal, unlike the RF signal, cannot pass through barriers, preventing eavesdropping [9].

An FSO communication system, on the other hand, has some disadvantages. Due to its short beamwidth, it necessitates precise alignment and pointing. A clear LOS between the transmitter and receiver is needed because the light cannot penetrate the walls, hills, or buildings. Furthermore, FSO systems are highly vulnerable to atmospheric conditions, significantly limiting their performance. The sun's location concerning the laser transmitter and receiver is another limiting factor. Solar background radiations can increase in a specific alignment, resulting in poor system performance [10].

1.3 THE UAV APPLICATIONS

UAVs are a subset of aerial vehicles that play an essential role in constructing the interconnected space-air-ground network. UAVs may serve the consumers who do not have access to telecommunications, such as in disaster zones where ground network infrastructure has been lost, or supplement existing communications. In addition, the UAV serves as a relay between a satellite link and an end-user via a ground link [11].

Both military and civilian applications are possible with UAVs. The critical scenarios for using UAVs in the military are monitoring and detecting the battlefield, discovering strategic targets behind enemy lines, maintaining stability in sensitive areas, assisting troops, and bringing weapons useable items for supply. In addition, observing critical buildings such as airports, pipelines, bridges, dams, or traffic would be conceivable with UAV applications [7].

1.4 INTER-UAV LINK: CONFIGURATION AND CHALLENGES

The physical configuration of the inter-UAV connection is a guided LOS, which is a common configuration for point-to-point communication links, often outdoors. However, FSO is a difficult medium in general. Therefore, when designing high-speed FSO connections, several considerations must be studied, such as how light will be scattered and absorbed because of the metrological conditions [12].

Creating an FSO link with a moving node is a challenging task. If the moving object is a flying aircraft, the difficulty will become much more difficult due to the additional degrees of freedom that must be considered. The connection must be established before data can be transmitted via the FSO link. The role can be broken down into subtasks for pointing, acquisition, and tracking (PAT) subtasks. The pointing stage states the rough alignment link between the two FSO nodes. Precise adjustments occur during the acquisition phase, and optical communication can start. Simultaneously, the tracking phase starts to preserve the two FSO-nodes aligned, as mentioned by E. Leitgeb et al. [13].

The multipath-induced beam distortion in directed LOS connections with a limited field-of-view (FOV) receiver is almost non-existent, and the noise from ambient sources is primarily rejected.

However, the free-space path loss limits the data rate. The LOS of the Optical Wireless Communication (OWC) link has many benefits, such as high data rates up to 100 Gb/s, security, a compact terminal size, lightweight, small aperture diameters, and power consumption is low. FSO links can offer a similar optical fiber communication performance over a link distance that ranges from a few hundred meters to several kilometers. The obtained signal fades more than the RF waves due to the atmospheric and weather conditions. Therefore, the transmitted power of the light beam can reach 100 mW, having enough receiver power margin to deal with attenuation caused by atmospheric and climatic circumstances [12].

1.4.1 Pointing Error in UAV Systems

UAVs link has an additional challenge: the moving link makes the alignment process one of UAVs-based FSO communication's critical issues. Most of the FSO pointing error research had been done to the fixed FSO link. However, the fixed link's pointing error can be extended to mobile or flexible FSO links.

The UAVs can generally run in a static mode or travel along a well-defined trajectory to assist the FSO source at the ground, relay, and destination terminals. In addition, the very heavy FSO transceivers can be carried by UAVs that follow a predetermined flight route. These requirements are met by UAVs with low altitude long endurance (LALE) and medium altitude long endurance (MALE), according to [14].

The stationary and moving UAV is subjected to atmospheric attenuation and other losses such as pointing loss, geometric loss, etc. For inter-UAV links, the references and research are limited for flexible FSO links, so they will be on the terrestrial FSO link pointing error and scaled up for inter-UAV FSO links.

1.5 UAV FEATURES AND CLASSIFICATION

The following are some of the features that set UAV communication apart from traditional communication:

a. Due to the UAV velocity, the characteristics of the communication networks for a slanted link (air-ground) and aerial link (air-air) propagations are highly dynamic.

b. Due to the movement of the aerial base station or the ground operators, non–stationary channels show severe spatial and temporal fluctuations.

c. The physical design and rotations of the UAV specify airframe shadowing, as mentioned by [15].

UAV size and configuration vary from one to the next. Total take-off weight, control autonomy, operational altitude, ownership, launch system, and airspace class are the most common factors to classify UAVs. UAVs were divided into four categories based on the action radius and cruise length: UAVs with a high elevation and long endurance, UAVs with a medium-range, small UAVs with a low cost and a short-range, and mini drones [16]. The UAV radius range is critical and classified in terms of the capability as:

A. Long endurance (the ability to endure for an extended period) UAVs are applied in exploration, interception, or attacks.
B. Middle-range UAVs have an achievement radius is 650 km nearly, designed for mid-range exploration or combat effect assessment.
C. Short-range and small UAVs have an achievement radius of less than 350 km, the altitude is less than 3 km, and the cruising duration is about 8-12 hours.
D. A close-range UAV has a shorter cruise range, ranging from 1 to 6 hours and depending on the mission, and afford a range of at least 30 km.
E. Close-range, low-cost UAVs can reach a height of roughly 5 km.
F. Consumer and commercial UAVs have a limited distance range. They can be operated by a remote control console or even an application installed on a smartphone or tablet computer, bringing the age of "drones" with immense commercial potential [16].

Given the wide variety of UAV categories, there is a clear distinction between UAV and commercial aerospace communications. In contrast, UAV and aerospace communications have a lot in common are:

i. Civil aerospace communication channel measurements are often performed by human-crewed aircraft, needing airports for taking off and landing. In addition, civil aerospace communication needs a sufficient elevation and a sufficiently long range to allow for little maneuvering. Finally, because most military or industrial UAVs are also located at airports, the aerospace channel would provide a foundation for UAV connection designs.
ii. The flight height of UAV communication channels varies depending on the aircraft size. For example, the mini-UAV range is tens of meters, while the UAVs take off from an airport and fly like an airplane and the distance range is thousands of meters. Forced turning maneuvering is possible with the former; the latter, on the other hand, can work under harsh situations, resulting in channels close to those used in the aerospace industry [16].

1.6 INFRASTRUCTURE OF THE UAV SYSTEM

An Unmanned Aerial System (UAS) is created by combining UAVs with base control stations on the ground and optical or RF links. UAS must be seen in the sense of a larger framework that involves the communication, command, and control (C3) system. Chaoxing et al. [15, p. 107769] suggested three main infrastructures to build a hybrid aerial mobile system "for the aerial networks of a space-air-ground integrated network, UAVs, airships, and balloons." Depending on the size of these three types, there are two classifications: high-altitude platforms (HAPs) for large UAVs, airships, balloons, and Low-Altitude Platforms (LAPs) for small drones. As UAV communication is a new technology, it is essential to define the channel to create communication links, which can be divided into two categories as [15, p. 107769] mentioned: "air-to-ground (A2G) communications and air-to-air (A2A) communications." The A2A links allow sharing of the map or sensor data amongst UAVs. In contrast, the A2G links provide mission data to the base station located on the ground for task control and display [18].

If two UAVs are in the system, both communication types (A2A and A2G) are point-to-point communication networks. However, suppose there are more than two UAVs. In that case, the communication network could be one of the known architecture networks that are: ring architecture, star architecture, mesh architecture, as demonstrated in [7], [18], and [19].

1.7 OPERATED SPECTRUM OF THE UAV

The RF spectrum used in a UAV communication system was classified into ranges. According to [15], "The International Civil Aviation Organization (ICAO) decides that UAV control and non-payload communication (CNPC) links must operate over a protected spectrum." Therefore, many organizations authorized the spectrum bands as Chaoxing et al. mentioned:

To regulate the UAV applications, the international telecommunication union (I-TU) has allowed certain portions of the L-band: 960 MHz-977 MHz and C-band: 5030 MHz-5091 MHz for UAS CNPC links. The Ku-band downlink: 10.95 GHz -12.75 GHz and uplink: 14.0 GHz -14.47 GHz, and Ka-band downlink: 19.70 GHz-20.20 GHz and uplink: 29.5 GHz-30 GHz are authorized for beyond-line-of-sight (BLOS) CNPC spectrum of satellite aeronautical safety communications. The bands 840.5 MHz-845 MHz, 1430 MHz-1444 MHz, and 2408 MHz-2440 MHz have been approved for unmanned aircraft systems relaying on LOS links by China [15, p. 107772].

While in FSO technology, there is no such spectrum classification for optical spectrum because the optical is licensed free.

1.8 THE LITERATURE REVIEW

The background on the performance of FSO link communication was started in the last two decades. Some of these researches studied the performance of the systems in different terms such as the outage probability, capacity, received power, or BER, by taking the effect of various issues such as atmospheric attenuation, atmospheric turbulence, misalignment, angle of arriving fluctuation, etc. These studies were done on different types of FSO links, such as terrestrial links (horizontal link), G2A or A2G links (slanted link), and deep space links such as inter-satellite and inter-UAVs links.

The literature review was divided into two parts due to the paucity of research considering the UAV-based FSO communication's pointing error. The first part is the pointing error for the terrestrial FSO link. The second part is the literature review on various UAV-based FSO link communication studies.

1.8.1 Literature Review on Pointing Errors for FSO Links

i. E. Bisaillon et al., in 2002. They recommended integrating an active alignment technique with an optimized optical architecture; the active alignment system utilizes a redundant collection of optical links and an active selection of the optimal connection. The aim is to encode a single channel within defined limits of lateral or angular misalignment. The optical system was utilized to improve the efficiency of power coupling between a 3×3 single-mode array of 960 nm and 3 μm diameter of vertical-cavity surface-emitting laser (VCSEL) type and a 250 m pitch and 3×3 photodetector array of 70μm diameter and 125μm pitch. The simulations were easier by considering the source and detector arrays' equilibrium. The results showed that the VCSEL-PD pair holds the coupling loss below 15 dB under lateral and angular misalignments, except in the worst-case misalignment. The receiver's sensitivity determined the tolerance for misalignment. For BER = 10^{-12}, the receiver bandwidth was between 18.5 and 750 Mb/s. The best sensitivity was obtained at a data rate = 450Mb/s, so this was chosen as the bit rate for the misalignment tolerance characterization. For a board separation of between 5 and 20 cm, the optical link achieved the desired misalignment of the lateral and angular toleration of ±1 mm and ±1°, respectively [20].

ii. Farid and Hranilovic, in 2007. They studied the effects of beamwidth, pointing error alteration, and detector size in a slow fading FSO channel. The modulation used was the On-Off Keying (OOK) technique (Intensity Modulation/Direct Detection (IM/DD). The measured performance was the power and outage probability using two types of distributions, lognormal and gamma-gamma distribution turbulence. In addition, they tried to increase the channel capacity by optimizing the beamwidth to face the weather condition and misalignment. The results verified that enhancing the beamwidth results in substantial rises in the channel capacity depending on the outage. Moreover, possible highest rates could be achieved using error-correcting codes that should be realistic and practical [21].

iii. Shlomi Arnon [20], 2003, stated that the transceivers placed on high-rise buildings are affected by many factors such as "dynamic wind-loads, thermal expansion, and weak earthquakes cause buildings to sway." Therefore, the designer should increase the transmitter beam divergence angle to decrease the influences and keep the LOS between the transmitter and the receiver. Nevertheless, an extensive divergence beam angle increases the beam's power, increasing the equipment cost and complexity. However, an excessively narrow beam divergence angle may cause communication to be cut off when a building sways. For the device, the author did not employ tracking and pointing mechanism. Instead, he assumed a large FOV receiver telescope so that the LOS to the transmitter was unaffected by building sway. The research aims to develop a mathematical model by lowering transmitted power and optimizing transmitter gain (divergence angle) as a function of building-sway statistics, the parameters of the communication system, and the required bit-error probability (BEP). The working model could decrease the required power by greater than 4 dB by comparing a system with half and twice the optimal divergence angle for a BEP of 10^{-9}. The result shows that a suitable divergence angle design is crucial for any practical system [22].

iv. Harilaos G. Sandalidis, in 2008. He considered an FSO channel affected by fading due to a pointing error. The system model assumption used is IM/DD with OOK modulation. The difference between this work and the reference [21] was that new closed-form formulations gave the BER and outage probability. Four optimization models have been developed and solved, with various metrics such as beamwidth, SNR, normalized jitter, BER, and outage probability is taken into account [23]. The similarity between [21] and this work was that the author here assumed "a Gaussian spatial intensity profile of beam waist w_z (radius calculated at e^{-2}) on the receiver plane at distance z from the transmitter and a circular aperture of radius r" [21, p. 395].

v. Harilaos et al., in 2008. The K distribution was used in this work as a statistical FSO channel that combined the strong turbulence and misalignment effect. The light beam was modulated using IM/DD with OOK and transmitted through a K turbulence horizontal path with Additive White Gaussian Noise (AWGN) and the attendance of pointing errors. The photodetector's responsivity integrates the photocurrent signal produced at the receiver for each bit duration. A BER has been achieved by choosing an optimal beamwidth that reduces the required transmitting power. However, the optimization problem was complicated because the average BER and unique algorithms' complex derived formulae may be needed [24].

vi. Harilaos G. Sandalidis, in 2011. Error control coding schemes had been proposed for reliable communication within the practical range of SNR to reach the BER target. The convolutional coded OOK in strong turbulence in the presence of the pointing error effect using symbol-by-symbol interleaved channels to investigate the error performance in the FSO system. Furthermore, different channel types were considered, and the analytical expressions for the pointing error and BER (pairwise error probability (PEP)) were used. The K or Negative Exponential (NE) distributions model was used to express the turbulence of the channel. The misalignment fading had been characterized by a distribution proposed in [21]. The exact mathematical formulation of PEP is derived from various combinations of channels, assuming the effects of turbulence and pointing error. Using the transfer function technique, these formulas were used to get upper bounds on BER performance. The overall fading was assumed to stay static throughout one-bit interval (slow fading channel) and independently alter from one interval to another. Perfect interleaving and de-interleaving are used at the transmitter and receiver, respectively. The interleaving and de-interleaving function together to create fades that are not based on a symbol to a symbol. However, complete interleaving involves big interleaves in the range of giga-symbols. This assumption does not seem realistic today and may be valid in future systems. Therefore, this research is considered a benchmark for a further practical quasi-static channel, in which the beam intensity stays static over a block of symbols. The study examined the following cases:

   a. K channel.
   b. Negative-Exponential (NE) channel.
   c. Pointing Error (PE) channel.
   d. K+PE channel.
   e. NE+PE channel.

The numerical results examined the performance of the interleaved symbol by symbol channel under turbulence and misalignment fading situations. The results showed that it could achieve a tiny BER target for a slight SNR value by error control coding, satisfying today's communication demands [25].

vii. Shijian Tang and et al., in 2012. This study investigated and simulated the misalignment of the underwater wireless communication optical link with a narrow divergence light source and presented an expression of the relationship between link distance, transmitted power, and receiver offset distance. The authors simulated light scattering by many particles hanging in the seawater and verified the tremendous influence on the light beam propagation, mainly in coastal and harbor environments. As a result, a diffuse light beam is gradually shaped as the link distance increases, replacing the source's collimated laser field. The irradiance distribution called beam-spread function was used to model the optical channel. This model has been used since the underwater environment has small-angle scattering properties; light scatters essentially at relative forward angles. The maximum likelihood (ML) scheme was used to detect the signal at the receiver. As the transmitted power increased, the BER decreased for a fixed offset and vice versa. That is logical because fewer photons were detected when the receiver was not aligned with the link. As a result, the received signal's minimum power was identified, lowering the overall performance. When setting the BER threshold=10^{-4}, diverse transmitted power permits the receiver for a specific offset distance. Numerical results suggest that the receiver's appropriate offset distance was allowed with a particular transmitted power and link distance regardless of water types [26].

viii. E. Lee et al., 2012. The FSO link's outage probability and average channel power were calculated using a combination of slow-fading channel and Gaussian beam wave models. Due to the averaging aperture effect, the study found that a larger receiver aperture could result in a lower outage probability. The best way to optimize capacity metrics is to choose the aperture size and beamwidth for a known wavelength for long path connections and strong turbulence situations. Various connection design parameters were considered to observe the system's characteristics under various scenarios. Also, capacity optimization is best performed by selecting aperture and beamwidth for a known wavelength and increasing the transmitted power. A complete system outage happened under the light fog situation at link distances more than 1.5km and was non-recoverable, optimizing the system parameters [27].

ix. Nazmi A. Mohammed et al., 2012. A pointing error assessment for practical BER had been carried out. The work was done for an FSO link under various weather conditions at 1.55μm. The maximum permissible pointing error for the FSO link under various weather conditions for fixed practical BER was estimated. The simulation has been done by MATLAB 2008 & Optisystem 7.0. Many factors in determining the FSO link's performance include link distance, laser wavelength, laser modulators, types of detectors, and efficiencies of transmitters and receivers. Also, they set the atmospheric attenuation factors and FSO system specifications such as types of lasers applied in the transmitters, the type of the receiver's detectors, the efficiencies of the transmitter and receiver. Using MATLAB, the numerical results revealed that the attenuation factor was 0.155dB/km for clear air. The attenuation factor increased to 84.904dB/km for the heavy fog, agreeing with the decreasing visibility of weather conditions. In Optisystem 7.0, establish an FSO link based on the previous mathematical model fed by system requirements. The results showed that the range of maximum pointing errors allowed to ensure BER not greater than 10^{-9} is in the range of 10's micro radians for clear and haze weather conditions. In the case of moderate fog, the range had been decreased. Finally, there was no allowance of any pointing error in the transmitter or the receiver under the previously mentioned design specifications and BER for heavy fog. The previous observations were due to the exponential nature of the pointing error loss and the narrow beamwidth of the used laser sources in FSO links. Both reasons make any minimal misalignment cause significant power loss and exceed the preferred threshold BER, reducing the range of allowable pointing error. Also, a slight increase in the pointing error led to a significant reduction in the received optical power, indicating the pointing error's binding effect in designing FSO links. They mentioned some suggestions to overcome these problems. The designer suggests auto-tracking methods, narrow and high-power transmitted beams, high-sensitivity receivers, and accurate weather monitoring [28].

x. Md. Tawabur et al. in 2012. They have investigated the FSO system's performance by considering three factors: pointing error, the atmosphere's turbulence, and path loss. First, the suggested FSO system was studied using MATLAB Simulink, where the free space was used as a channel. Then, it measured BER performance with various parameters such as link distance, transmitted and received signal power, path loss, and atmospheric turbulence. Finally, they decided to carry out the proposed system depending on the results. For the link distance between 100m to 500m, the output magnitude had been reduced beyond 500m drastically. Furthermore, the calculated BER showed that it is affected inversely with the transmitted power (increase transmitted power decrease BER); also, it is affected inversely by the path loss factor [29].

xi. Imran Shafique et al., in 2013. They evaluated the performance of a dual-hop relaying transmission system with asymmetrical RF/FSO links and pointing errors. The system model is similar to the model used in [30]. The probability distribution function (PDF), cumulative distribution function (CDF), instants end-to-end SNR, and instant generating function were derived using Meijer's G function. They used their findings to create new precise closed-form equations for higher-order fading, average error rates for binary and M-ary schemes, and ergodic power, all defined in terms of Meijer's G functions. The results from the computer-based Monte-Carlo simulation were used to verify the most recent analytical results [31].

xii. Juraj Poliak and et al., in 2013 [32]. Three cases of misalignment were discussed; each has its analysis and influence on the link behavior. They concentrated on examining the impact of different misalignments on obtained power. The mathematical expression for the impact of different forms of misalignment on obtained power has been presented. Gaussian beam distribution of the transmitted beam had been considered. The simulated results were developed using MATLAB. The received power has additional attenuation analysis of different misalignments. According to the results, the most crucial misalignment in the system sensitivity was the transmitter tilt. Wide beamwidth should be selected to decrease the system's sensitivity to the transmitter tilt; however, the received power worsens. The authors suggested that a trade-off for each specific system between the transmitter tilt's sensitivity and the received power (with additional attenuation due to lateral misalignment) be determined [32].

xiii. Jan Vitasek et al., in 2014. They described losses such as misalignment in the FSO link originating from incorrect installation of FSO terminals. The computation of misalignment loss was done for professional equipment set up on the roof of one building in the technical university of Ostrava and based on the power budget. Three transmitters mount each FSO head with a total optical power of 140 mW. The transmitted wavelength was 830-860 nm and two mrad beam divergence. The transmitter lens diameter was 6cm, the receiver lens diameter was 20 cm. The receiver's sensitivity was -33 dBm, the receiver operating range was from 0 to -17 dBm. The distance between the FSO heads was 1.47 km. In place of the receiver FSO head, the optical intensity transmitted from the opposite FSO head was measured. The measuring device was used to measure the intensity distribution. Stepper motors enable the device to move in two axes. The device's long armrest was 180cm; therefore, part of the maximum optical intensity distribution was measured in the x-axis direction.

The Gaussian function described the transmitted beam. The "*cftool"* function in MATLAB, the interpolation of measured data, was done to obtain a formula describing optical intensity distribution. The results showed that the somewhat slight misalignment causes significant increases in misalignment loss. FSO heads' distance was significant; the misalignment could seem effortless when the distance increased. Thus, the accurateness of alignment was critical for long-distance. The source for misalignment loss could be a high wind blow. Thus, a high-quality and robust mounting device for FSO heads is needed [33].

xiiii. Yuan Jiao and et al., in 2015. Their system model consists of multi-hop FSO communication. They determined the outage probability when the system was impaired by weak turbulence and misalignment. The authors used the decode-and-forward (DF) technique and derived the closed-form analytical formula for the serial end-to-end. The multi-hop technique was used to solve the disappointing performance of long-distance links. Three fading factors that affect FSO links are considered in their paper: turbulence effect, path-loss, and pointing errors. This work is similar to reference [21], but N points before the light arrive at the destination, as shown in Figure 1.3.

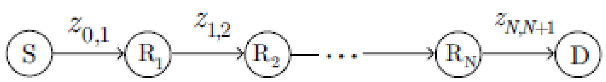

Figure 1.3: N points FSO communication system [21]

IM/DD OOK was used as a modulation technique. The aperture size of the detector, beamwidth, and jitter variance was taken into account to derive a statistical model for pointing errors. Rayleigh distribution has been considered at the receiver as the radial displacement.

The simulation results at weak turbulence (light fog) with a visibility of 1km set the FSO communication system's parameters and assumed the consecutive nodes are the equidistant route. Thus, the power transmitted from each node was equal. The results showed that the performance in terms of outage probability versus the receiving radius for different relay nodes decreases when the receiver radius increase. Meanwhile, when the number of relay node increase, the outage probability decreases. The analytical results were similar to the simulation results, and the differences were minimal and neglected.

Furthermore, when outage probability was compared to total connection distance with different relay nodes, the results revealed that the outage probability increased as total connection distance increased. Therefore, the serial multi-hop with DF transmission is appropriate for increasing the total link distance and the FSO communications' performance. The authors concluded that the worse performance occurred when the pointing error and the overall link distance increased. They mitigate this issue when using more relay nodes [34].

xiv. Govardhani Immadi et al., in 2017. They designed an FSO system with multiple transceivers (applying the spatial diversity and pre-amplification techniques) of four transmitters &

receivers and analyzed the Q-factor, BER, beam divergence, and received power with different climate conditions of clear air, haze, moderate to light fog at wavelength 850 nm and 1550 nm. The results showed that the receiver's received power decreased as the beam divergence increased. So, fewer divergence values get more receiving power [35].

The studies on [9] and [36] had dealt with the pointing error problems, and [37] was attempted to reduce the pointing error. The details are mentioned in the next sections.

1.8.2 Literature Review For UAV-Based FSO Communication

Setup aerial communication links have been an attractive topic for researchers in the past. HAP is one of the aerial link applications that has gotten a great deal of attention. UAV-based FSO communication is similar to HAP, with a fundamental difference regarding the communication channel's characteristics. The research on UAV-based FSO communications is recent, primarily, measurement of UAV communication link performance in terms of BER by tacking the effect of pointing error. Many researchers have studied the literature on UAV-based FSO links listed below.

i. Alan Harris et al., in 2005. They investigated two things: the ability of the motorized gimbal to execute alignment and track an FSO link between the UAV and base station. The gimbal's repeatability and accuracy were measured experimentally to validate that the station-UAV link was tracked and aligned.

ii. The second part was the simulation portion investigating the divergence quantity existing in the light beam when the laser beam's turbulence and scintillation index existed and the signal fading probability under a required threshold. The simulations were done using the ALTM program (atmospheric laser turbulence model) from ONTAR Company. The simulation was considered a link-state where the UAV follows a circular route with a radius of 4km and an altitude of 4km. The output power from the transmitter was 20 mW and had a wavelength of 1550 nm.

iii. Simulated results demonstrated that the divergence influences result in a beam profile that effectively offsets repeatability and accuracy. Finally, the predictable geometric loss for a station-UAV not be a restriction factor in the link performance [38].

iv. Ch. Chlestil et al. in 2006. This paper investigated how to maintain high-performance and reliable wireless communication between UAV swarms that benefit from the FSO links' high data rate. The study explained different UAV swarms networking architectures. The transmitted data between airbornes terminals using collimated laser beam has sight loss, disturbances in the atmosphere, and geometrical losses. Also, they limited the link distance between UAVs to 3km to increase the link's reliability and availability.

v. They depended on simulation results that were done before this study. The results showed that for a 1km distance between UAVs, the divergence angle of 50mrad needs a transmitted power of 11mW for clear weather. At temperate fog conditions, the needed transmitted power was 113 mW. At a 2km distance, the needed transmitted power increased to 44 mW for clear sky and 4.6 W in fog weather conditions. They suggested a solution to overcome the drawbacks of LOS for FSO links on mobile platforms without using high-priced tracking turrets. They studied unamendable laser stands on UAVs using spherical and highly directional emitters with a significant stream of light divergence.

vi. They concluded that the benefit of using this technique is that the FSO UAV swarms could arrive at the operation region without transmitting RF signals; therefore, these constructions were not discovered by radio scrutiny. The UAVs could use their extra RF communication tools during a short observation and monitoring mission at the target area or throughout an attack [7].

vii. S. Sheikh Muhammad et al. in 2006. This survey paper highlighted the challenge of maintaining a LOS FSO link of the UAV swarm scenario caused by the continuous movement and altering of the relative speed of participant's members. They invoked the challenges of employing FSO in the UAV swarm. The study mentioned two FSO links, ground-to-UAV, and inter-UAV links, and how to keep the FSO link active. The factors pitch, roll, and yaw combined with rotation and translation must be monitored and processed continually. To solve the rotation issues, calculate, know, and guess the single UAV's roll, yaw, and pitch to preserve the FSO terminal stability. Then, it must be translated into appropriate coordinates for aligning the FSO devices. The drawback was getting the precise position information for the flying vehicle. Hence, a requirement to employ an autonomous stand-alone system that is not dependent on other techniques than optics or to use a system that uses RF techniques such as GPS; but eliminates all of the optical system's advantages, particularly the non-detectable FSO signals. This study was reviewed in reference [38] also.

viii. Another cruel scenario of UAV swarms mentioned in this research was that the acquisition, tracking, and pointing of FSO links provide a considerable challenge. The UAV's stability depends on its weight and size. A technically challenging requirement limiting the technology's practical deployment is maintaining a LOS FSO link amongst flying UAVs that may experience relative motion among themselves. The UAV needs to exchange precise information about its position before taking off and through the flight with a reciprocal RF link or a GPS terminal.

ix. Moreover, they mentioned another method: scanning mirrors to steer the light beams between UAVs. A wafer bonding process had been used to create one and two-axis scanning mirrors, which would increase the reliability and security of the FSO connections. Finally, they looked at several simulations and trials done in the field of flying vehicles. They concluded that the effectiveness of inter-UAVs FSO connections needs theoretically detailed and scientific studies to evolve for real-world demonstration and experimentation [39].

x. E. Leitgeb and et al. in 2007. Provided a review for applying FSO on UAV systems. They investigated the Ground-UAV and UAV-UAV links scenarios and the possible inter-UAV links scenario. Also, the paper discussed the impact of atmospheric turbulence on performance. The simulation results were for clear weather conditions. They stated several issues: temperature, link distance, UAV altitude, UAV speed, relative humidity, daytime, UAV's roll, pitch, yaw angle, etc. [13].

xi. Antonis Hatziefremidis et al. in 2013. They measured the performance of a non-static link between the fixed station and the UAV. The work focused on showing the scintillation index's influences and the received power with noise on the performance of the link. They divided the slanted link into small Gaussian-beam wave segments. The altitude of the UAV, the wavelength, and the atmospheric conditions were all factors in a comprehensive comparative analysis of different FSO configurations. A simulation analysis calculated the scintillation index and the Rytov variance by dividing the slanted link into small segments. The average of both SNR and BER were measured. The results showed BER degradation of the slanted link compared to a horizontal path for the same circumstances [40].

xii. Asaad Kaadan and et al. (2014) [41]. They analyzed hovering multirotor UAVs' first open loop alignment and stability. A modeling structure was created to accommodate multi-section optical transceiver arrays with various variables that could be studied and controlled (e.g., the size of the array, path distance, beam divergence, wavelength, platform dynamics, others). Several simulated multirotor were used to evaluate the alignment model. Based on simulations, the commercial multirotor (MR) was ready for A2A FSO implementations with the proper optical array. Simulation platforms imitated the actual MR attitude and revealed 16% to 30% mutual alignment over a short distance. The goal of the work was to demonstrate the benefits of open-loop optical array designs while also providing a systematic methodology to quantify platform instability effects on FSO links. The findings could be incorporated into future closed-loop systems to improve tracking, alignment prediction, and trouble-free operation. They proposed two directions for future development: first, add curved transceiver arrays, laser-beam propagation models, and multi-cluster transmission patterns to expand the simulator. Second, continue to develop small, not heavy, and oversized FOV/FOR FSO technology, including fiber-bundle transceiver technology [41].

xiii. Wissam Fawaz et al., in 2018. The proposed FSO systems consist of relay-assisted to improve and remedy various atmospheric impairments effects on the optical signal quality. The conventional relay-assisted FSO was designed with two assumptions: buffer-free relays and immobile relays. These highly restrictive assumptions can be relaxed by incorporating UAV-assisted moving relays into conventional relay-assisted systems. Expressly, two scenarios of essential integration were provided and investigated by simulation. The simulation results indicate that the proposed considerably promising, creative, hybrid design has much promise. Furthermore, given that high-performance gains were observed under small buffer sizes, it is possible to utilize buffer-aided moving to relay UAVs to serve various purposes, including, for example, having these UAVs oversee the operation of amateur drones for potential misbehavior in the area of their deployment [13].

xiv. Mohammad Taghi et al., in 2018. They evaluated the benefits of MR UAV by using an accurate and computationally effective channel model. The statistical models were derived for the ground-UAV, UAV-UAV, and UAV-ground links over strong and weak atmospheric turbulence. The turbulence in the atmosphere and the position and angle-of-arrival fluctuations together were considered to determine the performance. The proposed analytical models were verified when comparing the numerically solved and the simulation results in the link outage probability.

xv. Furthermore, they discussed and considered various Tx/Rx parameters effect and optimized the link availability. As a result, the tunable Tx/Rx parameters (e.g., beam waist and FOV) get better performance, for example, the lowermost outage probability. The optimum parameters depend on channel cases such as link distance, the severity of turbulence, payload vibrations, transmitted power, and background noise [3].

xvi. Mohammad Taghi and Seyed Mohammad, in 2020. The letter aimed to derive the optimum UAV relay 3D coordinates and laser beam pattern by reducing the outage probability by describing source-relay and relay-destination channel models using a UAV-assisted FSO relay link. Moreover, they studied the effects of physical parameters (e.g., the UAV fluctuations direction strength, altitude, and obstacles location) on the UAV relay's optimum location. The findings demonstrated the importance of obtaining the best values for the adjustable parameters in the issue and how the physical factors of a specific region and the UAV's instability influenced the best UAV location [42].

1.9 THE PROBLEM STATEMENT

The proposed system consists of many drones (low-altitude UAV type). The drones continuously change their altitude h, link distance Z, and zenith angle θ, as stated in Eq. (1). Therefore, the pointing error factor H_p is a deterministic impairment in such types of systems. The previous work done by Wamidh et al. [4] considered the channel gain H that consists of two factors: the atmospheric attenuation H_a and the atmospheric turbulence H_f only. In this dissertation, the pointing error factor H_p and its related parameters are, the pointing error angle θ_r, and the link distance Z were considered to examine its role in system performance.

1.10 THE HYPOTHESISES

The assumptions considered when designing the proposed system are:

a. The drones' speed was considered constant (constant moving), and it changed its height simultaneously.

b. The movement of the drones in the range between 10° to less than 90°.

c. Varying the pointing error angle θ_r to measure the permitted values at specific link distances Z.

d. Varying the link distances Z between the main drone D_M and the Ground Station (GS) to examine the applicable distance for the specified pointing error angle θ_r value.

1.11 THE OBJECTIVES

The dissertation's main objectives are:

a. Design an aerial FSO system consisting of five drones connected by SISO and MISO channels using different parameters for each channel. The configuration was used in the previous study [43]. The proposed configuration took the V-shape.

b. Measure the flying system performance when the system's optical channels exposure to the channel gain includes pointing error H_p factor. The H_p factor was not considered in the previous study [43]

c. Measure and analyze the allowable range of the pointing error angles θ_r at specific link distance Z where the system gets high performance, and determine the link distances Z where the system failed at specific pointing error angle θ_r.

d. Measuring and comparing the SISO and MISO channels' performance and then for the system's overall performance in terms of ABER versus SNR.

2. THE FREE SPACE OPTICAL SYSTEM

2.1 FSO COMMUNICATION SYSTEM

FSO is a promising technology that can be applied in UAVs due to its easy installation, long link distance and duplex operation, high bandwidth, and more security. However, the main issue facing FSO communication is the light attenuation resulting from several atmospheric losses [44], such as atmospheric turbulence and attenuation, pointing error, geometrical loss, etcetera. FSO is a branch of Wireless Optical Communication (WOC).

WOC was classified into two general categories, indoor and outdoor WOC, as depicted in Figure 2.1 [45]. The indoor category was classified into four general configurations: non-directed LOS, directed LOS, quasi diffused, and diffused. Non-directed connections, which do not need exact alignment between the transmitter and receiver, are preferred when using wireless infrared communication. LOS connections require an unobstructed channel for successful communication, whereas diffuse links rely on numerous optical pathways from surface reflections. The outdoor or so-called FSO system is classified into two systems terrestrial and space. The FSO communication generally includes directed LOS and point-to-point laser connections through the atmosphere. FSO communication across a few kilometers has been proven [46].

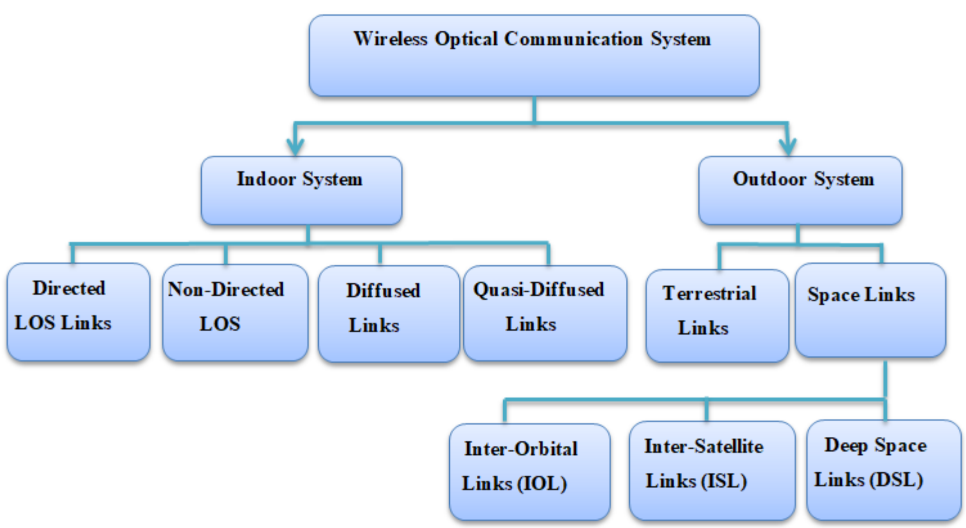

Figure 2.1: Wireless optical communication system classifications.

The applications of the outdoor WOC are last miles access networks, satellite/inter-satellite links, backup for fiber communication, disaster recovery, cellular communication backhaul, links under challenging terrains, local and wide area networks, terrestrial links (short or long-distances), and ground-air/air-ground links (UAV, HAP) [12].

FSO communication link includes three primary parts: transmitter, channel, and receiver, as shown in Figure 2.2 [10].

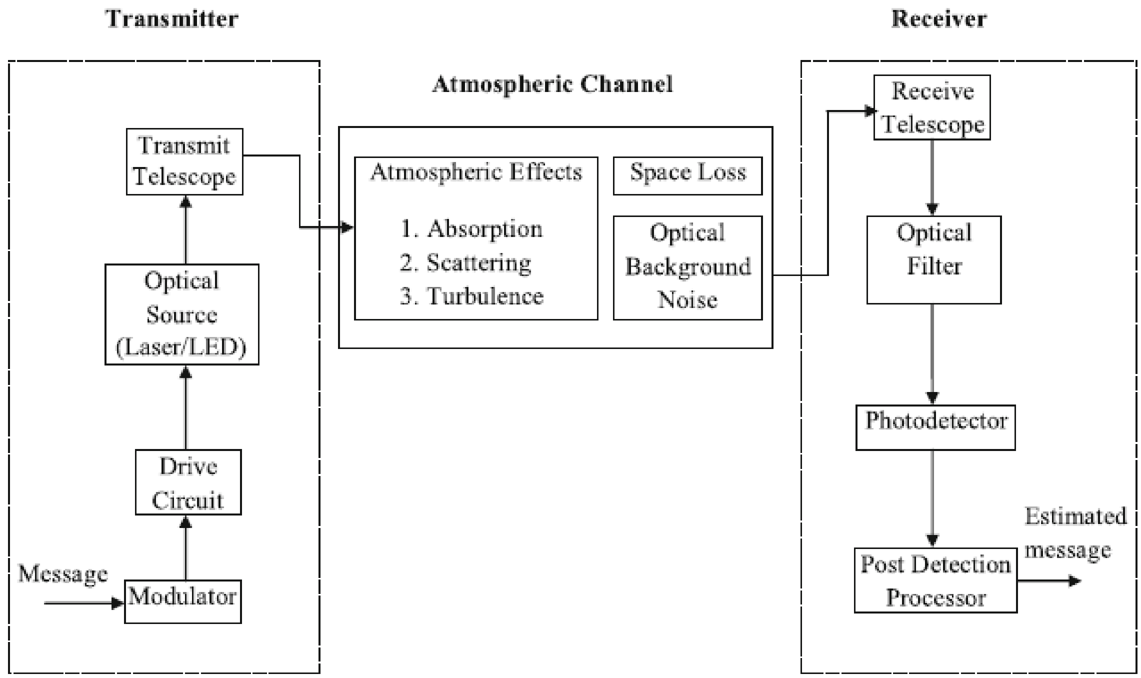

Figure 2.2: FSO communication link diagram [10]

A. The transmitter: The primary purpose of the transmitter is to modulate the message signal onto an optical carrier, which is subsequently sent to the receiver through the atmosphere. The transmitter's most essential components are:
   i. The modulator.
   ii. The optical source's driver circuit stabilizes the optical irradiation against temperature variations.
   iii. The telescope gathers, collimates, and guides optical light toward the receiver.
B. The channel: because the FSO link is propagated through the atmosphere, it is impacted by unforeseen environmental conditions such as clouds, snow, fog, rain, etc. The received

signal is attenuated and deteriorated due to variables that have no set features. Therefore, one of the limiting elements in the performance of the FSO link is the channel.

C. The receiver: the fundamental purpose of the receiver is to retrieve the sent data from incoming optical radiation. A receiver telescope, photodetector, optical filter, and demodulator system. The photodetector is collected and focused by the receiver telescope, which gathers and focuses the incoming optical radiation. The optical filter filters out background radiation and delivers the light to the photodetector, transforming the light into an electrical signal [10].

2.1.1 The Optical Sources and Wavelength Choice

The optical sources used for FSO transmission are Light-Emitting Diode (LED) or Laser Diode (LD). The optical spectrum wavelength for both sources extends from 700 to 10,000 nm. The basic requirements to select the laser are excellent conversion efficiency from electrical to optical, the quality of the laser, variable rate of repetition, regular operation, laser operation starts up quickly, and high reliability [10].

The outdoor laser's performance is exceptionally dependent on the wavelength. Because antenna gain is inversely related to the operating wavelength, it is more advantageous to operate at shorter wavelengths [9]. A shorter wavelength was used because the device and component were available at a low cost [12]. However, higher wavelengths offer enhanced link quality and low signal fades. For that reason, in the FSO link design, careful wavelength optimization helps achieve high performance. The wavelength selection is affected by many factors, such as the availability of transceiver components, cost, and eye safety guidelines. The International Commission on Illumination (ICI) classified the optical ray into three categories, as shown in [9]. The widely held FSO systems had been designed to operate in 780–850 nm and 1520–1600 nm windows. A beacon operating wavelength range used 780 nm to 1064nm. According to [47], the authors simulated and analyzed the appropriateness of three optical wavelengths are 850 nm, 1310 nm, and 1550 nm. They observed that the propagation distance was maximized under weak turbulence, and BER was minimized at 1550 nm wavelength. The 1550 nm wavelength is usually used as the operating wavelength because of the following:

i. Decrease Rayleigh scattering and background noise, where Rayleigh scattering coefficient has functional dependency as λ^{-4}. As a result, higher wavelengths exhibit trivial attenuation when compared to visible wavelengths.
ii. At 1550 nm, the transmitted power is 50 times more than at shorter wavelengths; therefore, it can overwhelm several losses caused by attenuation.
iii. At 1550 nm, the maximum permissible exposure (MPE) scale is much greater than at 850 nm, ensuring eye safety [45].

2.1.2 FSO Modulation Techniques

Different modulation techniques are appropriate for the FSO systems. The conventional FSO systems can use binary or multi-level modulation schemes, for which system design is cheap and straightforward [45]. The optical signal is modulated using amplitude, phase, frequency, or polarization. Comparing different techniques in the received power is necessary to obtain the preferred BER at a specific data rate. A power-efficient modulation scheme is appropriate to maximize the peak ratio to average power, as demonstrated by [48].

The OOK is the most modulation technique used. In addition, Pulse Position Modulation (PPM), Differential Pulse Shift Keying (DPSK), Differential Quadrature Pulse Shift Keying (DQPSK), and Subcarrier Intensity Modulation (SIM) techniques are used in FSO. OOK is the straightforward modulation scheme (as its design and implementation) in which the transmitter is ON only for the binary bit '1' and OFF for bit '0'. OOK modulation scheme is generally commercially available for FSO systems applications. However, besides its advantages, OOK is not an optimal modulation for the channels under turbulence conditions because turbulence directly affects the signal intensity. Moreover, it can be a sub-optimal technique if a fixed threshold is definite [49].

M-ary PPM is an appropriate technique for the direct detection photodetector. Some modulation techniques, such as PPM, exclude the input power decision threshold dependencies. Therefore it is a power-efficient modulation. The limitation is that it requires more bandwidth than OOK. PPM needs complex transmitter and receiver designs because of the high synchronization. Suppose we keep increasing M, the time slots through which an optical pulse occurs; the information transmitted per signal increases. Thus, higher transmission efficiency increases the required bandwidth by $M/\log_2 M$ times, which reduces band utilization efficiency. In M-PPM, more difficulties occurred to recover the symbol timing reference. DPSK has a benefit over OOK in that it has ~3db lower optical SNR required to obtain a given BER when using a balanced receiver. In OOK, the quantum is limited for an optical preamplifier receiver to 41 photons/bit; this decreases to 22 photons/bit when using a balanced detector. Therefore, it gives higher data rates over PPM and OOK with the receiver's complexity.

In DPSK, bandwidth decreases linearly with a decrease in data rates; thus, it is not suitable for the lower data rates. Also, its receiver needs an optical signal single-mode and free from phase noise, which decreases the efficiency of the signal's collection. Using a DPSK modulation scheme in atmospheric links without turbulence between satellites or air to satellite is limited due to all these limitations. When comparing the binary modulation schemes like OOK, DPSK with the DQPSK scheme duplicates the spectral efficiency by benefiting two signal quadratures of an optical carrier signal. In Subscriber intensity modulation (SIM), like PPM, it would not need the adaptive threshold without much bandwidth (like in PPM). However, the SIM gives poor power efficiency because it suffers from a high peak to average power ratio. Also, the non-linearity of the component is a big issue when dealing with multiple subcarriers. Therefore, the choice of the modulation schemes according to the application's requirements with some trade-offs among described factors [49].

2.1.3 FSO Atmospheric Channel Losses and Attenuation

The link's performance of the FSO is principally dependent upon the weather conditions and its installation location's physical characteristics. The link can operate at a field of two to three times the naked eye in any environmental condition.

2.1.3.1 Attenuation of the atmospheric

The atmospheric attenuation occurs because of several factors such as fog, clouds near the ground, rain, snow, dust, and different combinations of each, as demonstrated by [8] and [45]. The laser beam encountered various losses as transmitting over the atmospheric channel, such as:

2.1.3.2 The scattering and absorption losses

The light beam transmitted to the atmosphere interacts with different aerosols and gas molecules. The atmospheric channel's losses are primarily the results of absorption and scattering. Scattering and absorption are wavelength-dependent. Scattering and absorption of light are responsible for the performance of the FSO system degradation. Rayleigh scattering is used if the particles of the atmospheric size are small compared to the optical wavelength. The scattering is prominent around the visible or ultraviolet range, i.e., wavelengths lower than one μm. The scattering can be neglected at high wavelengths near the infrared (IR) range. If the size of the particle is comparable with the wavelength, Mie scattering is used. It is predominant near the IR wavelength and more prolonged. If the particles are more significant than the wavelength, such as the hail, rain, or snow, the geometrical optic models are used to describe the scattering [9]. The scattering process result is the optical beam's angular redistribution with and without wavelength change [45].

2.1.3.3 The atmospheric turbulence

Atmospheric turbulence is an arbitrary disturbance phenomenon due to the differences in temperature and pressure along the propagation path through the atmosphere. Three identified categories of atmospheric turbulence effects as the following:

i. Beam wanders arise when eddies are more significant than the light beam size. The wanders cause arbitrary beam deflection from its propagating path, resulting in link degradation. The wander of the beam is significant in uplink because the size of the light beam is more petite than eddies and result in displacement of the beam by many hundred meters. The Root Mean Square (RMS) of the light beam wanders displacement given as:

$$\sigma_{BW}^2 \approx 0.54(h_r - h_t)sec^2(\theta)\left(\frac{\lambda}{2W_0}\right)^2\left(\frac{2W_0}{\rho_0}\right)^{5/3} \tag{1.6}$$

where h_r and h_t are the receiver and transmitter altitude, respectively, ρ_0 is the coherence length of the atmosphere, θ is the zenith angle, λ is the wavelength, W_o is the initial beam size [9]. Wander leads to the beam's pointing error displacement, and that causes to miss the receiver [45].

ii. Beam spreading arises when the size of eddies is lesser than the size of a light beam. The light spreading causes the beam to be scattered and diffracted individually, resulting in the wavefront deformation and distortion of the received signal [9].

Light spreading results in a decrease in the density of the received power. However, the effect of the spreading will be insignificant when the diameter of the transmitted beam stay very small than the atmosphere coherence length or if the aperture diameter of the receiver stay more significant than the first Fresnel zone size $\sqrt{R/K}$. Therefore, the only effect will be beam wander and scintillation [45].

iii. Beam scintillation occurs if the size of eddies is in the order of the light beam size. Eddies act like a lens, focusing and defocusing the light beam. Therefore, the signal energy is redistributed in spatial and temporal irradiance fluctuations. The received signal-intensity fluctuations are scintillation and are the primary degradation source of the FSO system's performance [9]. In addition, scintillations cause loss of SNR, and deep random signal fades. Scintillation is decreased by employing multiple Tx/Rx antenna, aperture averaging, etc. [45].

The scintillation index, which is the normalized variance of intensity fluctuations σ_I^2, is used to quantify scintillation, given by:

$$\sigma_I^2 = \frac{\langle I^2 \rangle - \langle I \rangle^2}{\langle I \rangle^2} = \frac{\langle I^2 \rangle}{\langle I \rangle^2} - 1 \tag{1.7}$$

where I is the intensity at a particular point in the detector's plane and the angle brackets $\langle \quad \rangle$ refers to an ensemble average. The scintillation index is expressed as:

$$\sigma_I^2 = 4\sigma_x^2, \qquad \text{for } \sigma_x^2 << 1 \tag{1.8}$$

where σ_x^2 is the variance of log amplitude. The scintillation index is a function of a crucial parameter that is the refractive index structure parameter C_n^2. The value of C_n^2 determines the atmospheric turbulence strength and varies with daytime, geographical place, and altitude. The C_n^2 values for the horizontal link close to the ground are nearly constant. Depending on the strength of the turbulence, wherein weak turbulence, its expected value is 10^{-17} $m^{-3/2}$, and in strong turbulence, its value is greater than 10^{-13} $m^{-3/2}$. The value of C_n^2 for vertical links change with altitude h. When the altitude increases, C_n^2 decreases at a rate of $h^{-4/3}$. Therefore, the vertical link, C_n^2 must be integrated over the total link distance ranging from the receiver's height above sea level to the atmosphere top (approximately more than 40 km). Numerous empirical models of C_n^2 had been suggested to guess the turbulence profile by considering the experimental measurements executed at many geographical places, daytime, wind speeds, different types of terrain, etc. The Hufnagel-Valley Boundary (HVB) model is the furthermost model used for the vertical link is given as:

$$C_n^2(h) = 0.005940\left[\left(\frac{V}{27}\right)^2 (10^{-5}\times h)^{10}\, exp(-h/10^3) + 2.70\times 10^{-16} exp\left(-{}^{h}/_{1500}\right) + A\, exp\left(-{}^{h}/_{100}\right)\right]^{m^{-2/3}} \tag{1.9}$$

where V is the mean square value of the wind speed in m/s, and the parameter A can adjust its value to appropriate different site conditions is given as:

$$A = 1.29\times 10^{-12}\rho_0^{-5/3}\lambda^2 - 1.61\times 10^{-13}\theta_o^{-5/3}\lambda^2 + 3.89\times 10^{-15} \tag{1.10}$$

where θ_0 is the angular distance (isoplanatic angle in which turbulence remains constant), ρ_0 is the atmosphere coherence length that is a significant parameter depending on three parameters: the wavelength λ, C_n^2, and θ. The value of ρ_0 is dependent on whether the wave is plane or spherical.

Because of ρ_0 differs as $\lambda^{5/6}$, as a result, the link operating with a higher wavelength has a lesser influence amount of turbulence than at a lower wavelength. The scintillation index in weak atmospheric turbulence for a plane wave had been taken in terms of C_n^2 parameter as:

$$\sigma_I^2 = \sigma_R^2 \approx 2.240k^{7/6}(\sec(\theta))^{11/6}\int_{h_o}^{h_o+Z} C_n^2\,(h)h^{5/6}dh \tag{1.11}$$

k is the wavenumber ($2\pi/\lambda$), σ_R^2 the Rytov variance, and Z the distance of the link. In weak turbulence, i.e., $\sigma_I^2 < 1$, the intensity statistics are given by the lognormal distribution. In strong turbulence, $\sigma_I^2 \geq 1$, Rayleigh distribution is used. Several other models describe the scintillation statistic in strong turbulence, such as the *K* model or all the regimes such as *I-K*, *M*, and Gamma-Gamma models. The I-K model's expression is difficult to represent in closed form. The lognormal Rician distribution covered the weak and strong turbulence and applied if the light beam propagating through turbulence follows Rice-Nakagami statistics with lognormal. However, the numerical computation in a closed loop is less challenging to carry out. Therefore, the Gamma-Gamma model was used to characterize the scintillation statistic in weak and strong turbulence successfully. In the Gamma-Gamma distribution, the product of two independent arbitrary variables is the normalized irradiance I, i.e., $I = I_X I_Y$, where I_X and I_Y denote the large and small scale turbulent eddies, respectively. The Gamma-Gamma distribution of I is regulated by an independent Gamma model for each scale. The PDF of I is given by:

$$f_I(I) = \frac{2(\alpha\beta)^{(\alpha+\beta)/2}}{\Gamma(\alpha)\Gamma(\beta)} I^{((\alpha+\beta)/2)-1} \times K_{\alpha-\beta}\left(2\sqrt{\alpha\beta I}\right), \ \mathrm{I} > 0 \tag{1.12}$$

where $K_{\alpha}(\cdot)$ is the modified Bessel function of the second kind of order a. α and β parameters are the effective numbers of small and largescale eddies of the scattering atmosphere. For the gamma model, the scintillation index is expressed as:

$$\sigma_I^2 = \frac{E[I^2]}{(E[I])^2} - 1 = \frac{1}{\alpha} + \frac{1}{\beta} + \frac{1}{\alpha\beta} \tag{1.13}$$

The M-statistical model is a general distribution that unifies numerous current models used for atmospheric turbulence. Different models such as the lognormal, K, NE, Gamma-Gamma can be created using the unified M-distribution model [9].

2.1.3.4 The beam divergence loss

Light divergence arises as the light propagates through the air and results in diffraction close to the receiver and cause pointing error /geometrical losses; this is because the receiver gathers part of the transmitted beam. The losses increase as the length of the link increases, except that the receiver aperture size increases or implemented receiver diversity. The narrow beam of a light source with divergence is desirable. Conversely, narrow beam divergence results in link failure if a small pointing error occurs between the transmitter and receiver. For that reason, a suitable selection of beam divergence must be made to get rid of the need for an activity tracking and pointing system and reduce beam divergence loss [9].

2.1.3.5 The angle of arrival (AoA) fluctuations

The incoming light beam wavefront will be disfigured at the receiver because of the atmospheric turbulence. It leads to the image dancing or spot motion at the receiver focal plane. This phenomenon is known as angle of arrival (AoA) fluctuation. Adapting optics or a fast beam steering mirror have been used to compensate for the influence. The variance of AoA fluctuations, $\langle\beta^2\rangle$ is given as [9]:

$$\langle\beta^2\rangle = 2.91\left[\int_{h_0}^{H} C_n^2(h)dh\right] D_R^{-1/3} \sec(\theta) \quad (1.18)$$

which is further simplified to yield:

$$\langle\beta^2\rangle = 0.182\left(\frac{D_R}{\rho_0}\right)^{5/3}\left(\frac{\lambda}{D_R}\right)^2 \quad (1.19)$$

where the parameter D_R is the collecting lens diameter. The angle of arrival fluctuation $\langle\beta^2\rangle$ proportional inversely with the coherence length ρ_0 [9].

2.2 MISALIGNMENT OR POINTING ERROR

The loss result from improper alignment between transmitter and receiver is named pointing error [10]. The FSO's beam demands a high degree of directionality and a minimal beam divergence value. In addition, the used receiver in the FSO link has a restricted FOV. As a result, maintaining a consistent LOS connection between the transmitter and receiver is critical for ensuring 100% availability of FSO systems. The factors that cause pointing loss include platform instability and electronic and mechanical equipment stress. Also, the turbulence-induced wander can shift the beam from its transmit path and create the pointing error. The pointing error increases the opportunity of link failure or decreases the received power amount significantly, which produces a high error probability. Thus, the influence of pointing errors is significant on the FSO system performance [9].

The alignment of the links is critical for the proper functioning of the links. Therefore, the following status of misalignments was considered to evaluate their effect on the link activities:

A. The lateral misalignment Δ happens when the optical axis of the transmitted beam differs from that of the receiver. It can be visualized as a plane offset perpendicular to the propagation direction. The results of the lateral displacement and effects on the received signal analysis can determine the minimum distance between the receiver and the transmitter on one side of a bidirectional link so that reflected power does not affect the reception of the same user.

B. The transmitter aperture's tilt occurs when there is an angle between the transmitted beam axis and the connecting line of the transmitter-receivers; additional attenuation arises. As the angle increases, the received power decreases.

C. The receiver aperture's tilt occurs when tilted the receiver is from the angle's beam axis. However, the receiver aperture tilt has an insignificant influence and does not necessarily include in the link budget [32].

For each FSO link type, significant factors contribute to causing pointing errors to occur. For example, in the terrestrial fixed link (horizontal path), the factors that cause pointing errors: are building sway, wind loads, thermal expansion, earthquakes, etc. For slanted path links and deep-space links, the factors that cause the pointing error are the moving link, vibration or platform jitter, etc. The slanted link such as ground-to-satellite or ground-to-UAV and vice versa, while the deep-space links such as inter-satellite links, high altitude inter-UAVs links, and inter-HAP links. The common factors for pointing error occurring for these links are long-range FSO link, atmospheric attenuation, turbulence, transmitter's and receiver's mechanical displacement. Therefore, each FSO link has its characteristics and specifications.

The pointing error has an apparent dependence on the atmosphere's turbulence and is calculated in micro radians, determined in terms of attenuation [36]. In order to compensate for residual jitter, proper care must be taken to ensure that the platform is vibration-free. Proper bandwidth control and dynamic link distance are maintained to obtain a sub-micro-radian pointing exactitude [9]. The transmitter pointing loss that must be taken into account for the link budget is given:

$$L_p = exp\left(\frac{-8\theta_{jitter}^2}{\theta_{div}^2}\right) \tag{1.20}$$

where θ_{jitter} is the angle of the beam jitter, and θ_{div} is the divergence of the transmitter beam [10].

The calculation of the terrestrial FSO link's (horizontal link) pointing error is less complex than the calculation of deep space FSO and a slanted link, as shown in [36] and [37]. Figure 2.3 summarizes all the FSO link fading and losses.

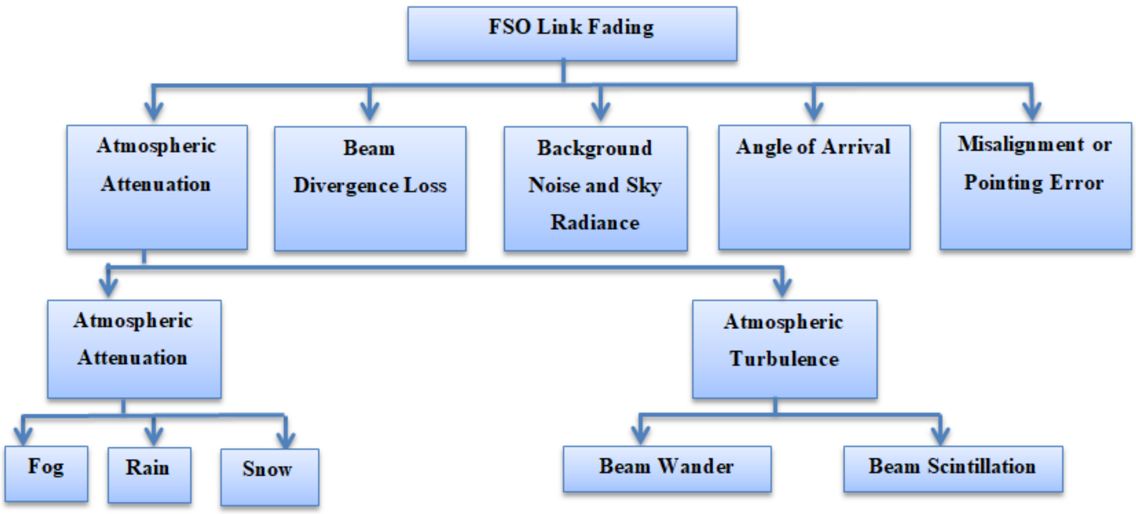

Figure 2.3: FSO Link Fading

2.3 FSO DETECTION TECHNIQUES

The photodetection techniques transform the received signal into an electrical signal. The conversion is done in the receiver's signal processing or decision-making unit. Photodetectors primarily extract the information embedded in the optical carrier signal (it may be embedded in the optical signal's frequency, phase, or intensity). In FSO systems, two common approaches are used for this purpose: coherent and direct detection. Here avalanche photodiode (APD) and PIN photodetectors have been used to detect the information bits. Photodetectors should have high sensitivity within their working wavelengths, low noise levels, appropriate bandwidth to hold the needed rates of data, the slightest effect on the response caused by temperature fluctuations, and lengthy operating life.

The coded signal is fed onto the atmosphere channels and reaches the destination. At the receiver, depending upon whether the local oscillator is used or not in the detection, the following detection techniques can be used:

A. Direct Detection.

B. Coherent Detection.

i. Heterodyne Detection.

ii. Homodyne Detection.

C. Maximum likelihood sequence detection (MLSD).

D. Iterative Detection [49].

Many standards define the most crucial compatibility and performance requests for detectors:

i. A large surface area of the detection means an extensive aperture collection and broader detection FOV. On the other hand, a small surface area of the photodetector arrays is the best possible option for high-speed applications.

ii. The photodetector has a high responsivity and sensitivity at the operating wavelength, low cost, compact size, and high level of reliability and dependability.

iii. High SNR because of low noise.

iv. Speedy response time.

The response speed and the photodetector bandwidth depend upon the photon-generated carrier's transit time through the depletion region; the electrical frequency response depends upon the diode's capacitance and the slow carrier's diffusion generated outside the depletion region [12].

There is another classification of photodetectors according to the applications. The detector's features are different and classified into communication and beacon detectors, as shown by Hemani et al. [45].

2.3.1 Photodetectors Types

Four different types of photodetectors could be implemented at the receiver side:

A. PIN photodetector (internal gain is absent, but a larger bandwidth compensates).

B. The APD photodetector.

C. The photoconductors.
D. The metal-semiconductor photodetectors.

Because they match all of the above characteristics, PIN and APD are the most extensively utilized in OWC systems [12].

2.3.1.1 PIN photodetector

The PIN photodetector contains two semiconductor materials, *p*-type and *n*-type, separated by a thin lamina of the n-doped intrinsic region. The device converts an incident beam into an electron/electric current. The energy of the incoming photon must not be less than the semiconductor material's band-gap energy. The responsivity of a PIN photodetector is less than unity. PIN photodetectors can operate at bit rates higher than 100 Gbps [12].

2.3.1.2 APD photodetector

The APD provides an inherent current gain through repetitive electron ionization, culminating in augmented sensitivity as the photocurrent is multiplied before the incident receiver circuit's thermal noise. The gain values are between 50~300; therefore, the APD responsivity value is above unity. The APD's drawback is that multiplication noise is always present because of the ionization/avalanche process's statistical nature, and APD has high sensitivity than the PIN photodetector. Also, the avalanche process is susceptible to temperature. These issues are necessary and should be considered when an APD is used in an FSO system [12].

3. SYSTEM AND CHANNEL MODELING

3.1 THE PROPOSED SYSTEM MODEL

The configuration of the proposed system of the flying drones is shown in Figure 3.1. It consists of several drones connected by optical links wirelessly and takes the V-shape. This type of configuration was mainly employed in [42] to discover and make profound decisions for specific area surveillance, but it did not consider the pointing error factor H_P. The system's optical channel's description consists of the SISO channel and MISO channel and can be clarified as the following:

A. The optical channel between the drones in both V-arms is the SISO channel (UAV-to-UAV SISO channel).

B. The optical channels between the drones in both V-arms (D_{11} and D_{12}) and the main drone D_M are considered the MISO channel (UAV-to-UAV MISO channel).

C. The drone D_M connected to the GS is considered the SISO channel (UAV-to-GS SISO channel).

D. The drone's overall link in both V-arms through the D_M to the GS is considered the SISO channel.

E. The ground station GS acts as a control station controlled by a human user to control and monitor the flying system.

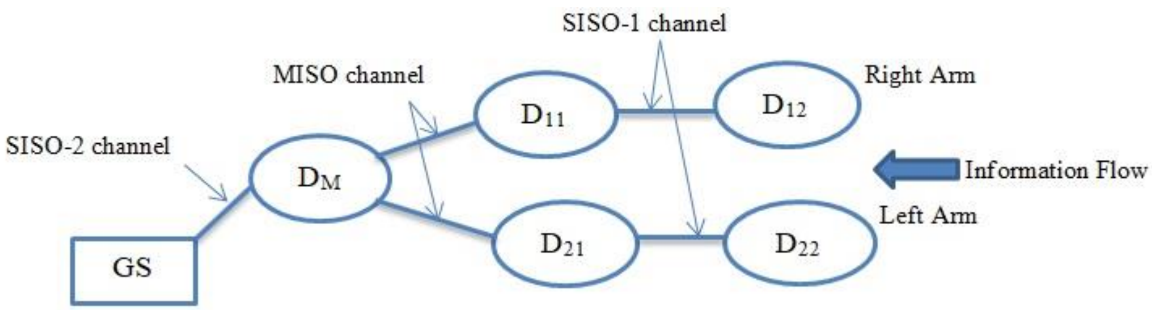

Figure 3.1: The V-shape configuration of drones FSO link.

The number of drones, the link distance between them, and the angle (the width) of the V-shape can be adjusted as needed to achieve the desired application. The optical signals from the drones in both arms to the D_M or D_M to the GS expose to the channel gain H. Additional parameters were considered when measuring the optical system performance. These parameters are the link distance *Z* between the drones or the distance between the D_M and the GS, the link zenith angle θ between the GS and D_M, and the pointing error angle θ_r. The system parameters are shown in Table 3.1.

Table 3.1: The system parameters

Parameter	Symbol	Value
Transmission Rate	R_0	1 Gbps
Optical Transmitted Power	P_t	40 mW (16 dBm)
Responsivity	*R*	1
Distance between Tx and Rx	*Z*	60~8000 m
Wavelength	λ	1550×10^{-9}nm
Receiver Diameter	D_R	1 cm to 10 cm
Pointing Error Angle	θ_r	Varying
Beam Waist at Z=0	w_0	5×10^{-2} cm

The beam waist w_0 is the width of the transmitted optical beam from the transmitter Tx. The receiver aperture D_R values are 1~ 10 cm and depend on the drone design and weight tolerance [18]. The purpose of increasing the receiver diameter is to increase their gathering efficiency by increasing the collected optical signal per centimeter. Increasing the aperture size, on the other hand, influences system performance. The operated wavelength λ is 1550 nm because it has a less attenuation transmission window (0.2 dB/km). The distance *Z* between two drones or between D_M and GS was assumed to vary and depend on the required test. The altitude *h* of the drones was assumed to be varied and depended on the drone datasheet's characteristics [51] and the specific test.

3.2 THE CHANNELS MODELING

The proposed system's mathematical expression includes the channel gain H with pointing error factor H_p and the probability distribution function (PDF) of H has been modeled. According to the previous assumptions, the flying system can be divided into three subsystems to measure its performance. The first subsystem is the UAV-UAV SISO-1 channel, the second is the UAV-UAV MISO channel, and the third is the UAV-GS SISO-2 channel. The first and second subsystems were considered as a horizontal link and the third subsystem as a slanted link in which the link distance Z change as the zenith angle θ or the altitude h change as given by Pythagoras's law:

$$Z = {}^{h}\!/_{\sin(\theta)} \tag{3.1}$$

The optical signals are modulated using a PPM signaling scheme and transmitted into the lognormal channel with AWGN. For the lognormal distribution, the scintillation index $\sigma_I^2 < 1$. The scintillation index σ_I^2 function is complicated and determined using the beam parameters, link distance, the transmitter and the receiver heights, and the refraction index n fluctuations. The primary source of scintillation is temperature differences in the index of refraction n, which is generally known as optical turbulence. The scintillation index σ_I^2 can be calculated as [52]:

$$\sigma_I^2 = \exp(\sigma_R^2) - 1 \tag{3.2}$$

where σ_R^2 is the lognormal variance (Rytov variance) that is given as:

$$\sigma_R^2 = 1.23\, C_n^2(h)\, K^{7/6}\, Z^{11/6} \tag{3.3}$$

$K = 2\pi/\lambda$ is the wavenumber of the optical. According to the scintillation value, three independent regimes depend on the Rytov variance: a weak regime, a moderate regime (focusing regime), and a strong regime (saturation regime). A suitable statistical model of the scintillation index for the three regimes was provided by the modified Rytov theory [53].

The optical signal was converted to an electrical signal at the receiver using a direct detection technique. The expected optical signal y at the receiver is expressed [24]:

$$y = HxR + n \tag{3.4}$$

x is the transmitted optical signal, R is the receiver responsivity, and depending on the photodetector type, n is the AWGN with variance $\sigma_n = N_0/2.0$, and H is the gain of the channel that is a composite of three factors and was expressed as [24]:

$$H = H_a H_f H_p \tag{3.5}$$

where H_a, H_f, and H_p are represent the attenuation result from the beam extinction due to absorption and scattering, scintillation impact, and geometric and pointing loss of the atmosphere channel, respectively. The behavior of the factor H_a does not show arbitrariness. Therefore, it is regarded as a deterministic factor with an extended period on the scale of hours compared to the bit durations in the nanoseconds or less range. On the other hand, H_f and H_p factors are variable in time that exhibit millisecond-scale fluctuations in the fading channel [37]. Beer-Lambert law modeled the H_a and expressed as [29]:

$$H_a = exp(-Z\sigma) \tag{3.6}$$

σ is the attenuation coefficient, which depends on visibility [3]. The atmospheric turbulence H_f is the channel fading was expressed as [29]:

$$H_f = \frac{2P_r}{\pi W} \tag{3.7}$$

where P_r is optical power received by the photodetector, W is a beam spot radius. The H_p factor is the optical beam pointing error and expressed as [29]:

$$H_p = A_0 exp\left(\frac{-2r^2}{W_{zeq}^2}\right) \tag{3.8}$$

where r is the beam radial displacement, and $A_0 = [erf(v)]^2$ is the part of gathered power at the radial displacement $r = 0$ (no pointing error occurs). The radial displacement $r = Z.\theta_r$ is between the center of the aperture and the center of the optical beam, as shown in Figure 3.2, where θ_r is pointing error angle (divergence angle) that must be $\leq 10^{-4}$ [5]. This value is for an extended link distance, such as the satellite links. For short-distance applications, the pointing error angle θ_r can be set $> 10^{-4}$ as proved in the results section.

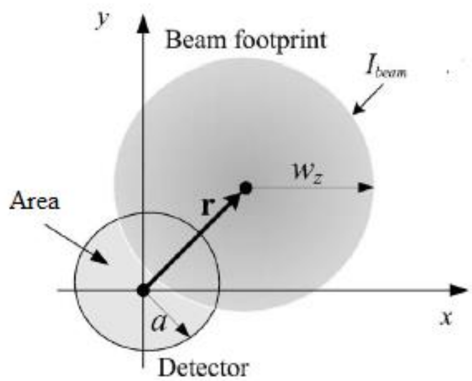

Figure 3.2: Beam footprint with detector plane misalignment [21].

The equivalent optical beam radius W_{zeq} can be expressed as [29]:

$$W_{zeq} = w_z^2 \frac{\sqrt{\pi} erf(v)}{2v\, exp(-v^2)} \tag{3.9}$$

where w_z is the beam radius when the irradiance drops to e^{-2} (0.135) at the distance Z of the axial value and is associated with the beam waist w_0 as:

$$w_z \approx w_0 \left[1 + \varepsilon \left(\frac{\lambda Z}{\pi w_0^2}\right)^2\right]^{\frac{1}{2}} \tag{3.10}$$

where $\varepsilon = (1 + 2w_0^2/\rho_0^2(Z))$, and the coherence length $\rho_0(Z) = (0.55C_n^2(h)K^2Z)^{-3/5}$, and $v = (\sqrt{\pi}\, a)/(\sqrt{2}\, w_z)$, where a is the receiver radius [21]. The Gaussian beam model validation requires $w_0 > (2\lambda/\pi)$ [5]. The PDF of the channel gain H in weak turbulence regime can be found after the derivative in [21] as:

$$f_H(H; wz) = \frac{\gamma^2}{2(A_0 H_a)^{\gamma^2}} H^{\gamma^2 - 1} \times erfc\left(\frac{ln\left(\frac{H}{A_0 H_a}\right) + \mu}{\sqrt{8}\sigma_x}\right) e^{\left(2\sigma_x^2 \gamma^2 (1+\gamma^2)\right)} \tag{3.11}$$

where $\gamma = \frac{W_{zeq}}{2\sigma_s}$, σ_s is the displacement standard deviation of the pointing error at the receiver,

$\mu = 2\sigma_x^2(1.0 + 2\gamma^2)$, and σ_x is the variance of the log amplitude that can be calculated depending on the wave shape plane and spherical [54]:

$$\sigma_x^2 = 0.30545\, K^{7/6}\, C_n^2(h) Z^{11/6} \approx \frac{\sigma_R^2}{4} \qquad \text{For plane-wave} \tag{3.12}$$

$$\sigma_x^2 = 0.3124\, K^{7/6}\, C_n^2(h) Z^{11/6} \qquad \text{For spherical wave} \tag{3.13}$$

For each channel of the proposed system, the channel gain H and its factors and the parameters related to it were measured independently, as shown in the next section. The channel's PDF gain for each subsystem's channel will be private to the specific channel.

3.2.1 UAV-UAV SISO-1 Channels Modeling

The SISO topology has `a single transmitting aperture and a single receiving aperture [55]. Two UAV-UAV SISO-1 channels are the left arm and right arm. The distance Z between two drones in the same arm, such as between D_{11} and D_{12} in the right arm, can be considered varying or fixed. The received optical signal y_{SISO}^{uu} can be expressed as:

$$y_{SISO}^{uu} = H_{SISO}^{uu} xR + n \tag{3.14}$$

where $\mathrm{H}_{\mathrm{SISO}}^{\mathrm{uu}}$ is the channel gain of the UAV-UAV SISO-1 topology that can be found by:

$$H_{SISO}^{uu} = H_{a_{SISO}}^{uu}\, H_{f_{SISO}}^{uu}\, H_{p_{SISO}}^{uu} \tag{3.15}$$

where $H_{a_{SISO}}^{uu}$, $H_{f_{SISO}}^{uu}$, and $H_{p_{SISO}}^{uu}$ represent the attenuation result from the beam extinction due to absorption and scattering, scintillation impact, and geometric and pointing loss of the atmosphere channel, respectively, of the UAV-UAV SISO-1 channel. $H_{a_{SISO}}^{uu}$ was modeled by Beer-Lambert law $H_{a_{SISO}}^{uu} = exp(-Z_{SISO}^{uu}\sigma)$, where Z_{SISO}^{uu} is the link distance between two drones in an arm. The atmospheric fading $H_{f_{SISO}}^{uu}$ can be expressed as:

$$H_{f_{SISO}}^{uu} = \frac{2Pr_{SISO}^{uu}}{\pi W_{SISO}^{uu}} \tag{3.16}$$

where ${P_r}_{SISO}^{uu}$ is the received power, and W_{SISO}^{uu} is beam spot radius at the receiver for the UAV-UAV SISO-1 channel, which can be calculated as:

$$W_{SISO}^{uu} = w_0({\theta_0}_{SISO}^{2^{uu}} + {\Lambda_0}_{SISO}^{2^{uu}}) \tag{3.17}$$

where w_0 is the beam waist at $Z_{SISO}^{uu} = 0$, ${\theta_0}_{SISO}^{uu} = \frac{1-Z_{SISO}^{uu}}{F_0}$ is the curvature factor, ${\Lambda_0}_{SISO}^{uu} = \frac{2Z_{SISO}^{uu}}{Kw_0^2}$ is Fresnel ratio, and the factor F_0 is the curvature radius. The pointing error ${H_p}_{SISO}^{uu}$ can be expressed as:

$${H_p}_{SISO}^{uu} = {A_0}_{SISO}^{uu} \exp\left(\frac{-2r_{SISO}^{uu}}{{W_{zeq}}_{SISO}^{2^{uu}}}\right) \tag{3.18}$$

where ${A_0}_{SISO}^{uu}$ is the part of the gathered power at Z_{SISO}^{uu}= 0, $r_{SISO}^{uu} = Z_{SISO}^{uu}.{\theta_r}_{SISO}^{uu}$ is the optical beam radial displacement, and ${W_{zeq}}_{SISO}^{uu} = w_{z_{SISO}}^{2^{uu}} \frac{\sqrt{\pi} erf(v)}{2v\ exp(-v^2)}$ is the equivalent beam radius for the UAV-UAV SISO-1 channel, $w_{z_{SISO}}^{uu}$ is the beam radius when the irradiance drops to e^{-2} of the axial value at a distance Z_{SISO}^{uu}, and is associated with the beam waist w_0 as:

$$w_{z_{SISO}}^{uu} \approx w_0 \left[1 + \varepsilon_{SISO}^{uu}\left(\frac{\lambda Z_{SISO}^{uu}}{\pi w_0^2}\right)^2\right]^{\frac{1}{2}} \tag{3.19}$$

where $\varepsilon_{SISO}^{uu} = (1 + 2w_0^2/\rho_0^2(Z_{SISO}^{uu}))$, $\rho_0(Z_{SISO}^{uu}) = (0.55C_n^2(h)K^2 Z_{SISO}^{uu})^{-3/5}$ is the coherence length, and $v_{SISO}^{uu} = (\sqrt{\pi}\, a) / (\sqrt{2}\ w_{z_{SISO}}^{uu})$, where a is the receiver radius.

Considering ${H_a}_{SISO}^{uu}$ as a stable scaling factor, the turbulence and misalignment-induced fading models are combined statistically [37]. Channel gain's PDF of H_{SISO}^{uu} can be expressed as:

$$f_{H_{SISO}^{uu}}(H_{SISO}^{uu}; \mathrm{w}_{z_{SISO}}^{uu}) = \int f_{H_{SISO}^{uu}|{H_f}_{SISO}^{uu}}\left(H_{SISO}^{uu}\middle|{H_f}_{SISO}^{uu}\right) f_{{H_f}_{SISO}^{uu}}\left({H_f}_{SISO}^{uu}\right) d{H_f}_{SISO}^{uu} \tag{3.20}$$

where $f_{H_{SISO}^{uu}}(H_{SISO}^{uu}; w_{z_{SISO}}^{uu})$ indicates to the PDFs group parameterized by the beamwidth $w_{z_{SISO}}^{uu}$, and $f_{H_{SISO}^{uu}|{H_f}_{SISO}^{uu}}\left(H_{SISO}^{uu}\middle|{H_f}_{SISO}^{uu}\right)$ is the conditional probability given the state of the turbulence ${H_f}_{SISO}^{uu}$ and expressed as:

$$f_{H_{SISO}^{uu}|H_{f\,SISO}^{\;uu}}\left(H_{SISO}^{uu}\middle|H_{f\,SISO}^{\;uu}\right)=\frac{1}{H_{f\,SISO}^{\;uu}\;H_{a\,SISO}^{\;uu}}f_{H_{p\,SISO}^{\;uu}}\left(\frac{H_{SISO}^{uu}}{H_{f\,SISO}^{\;uu}\;H_{a\,SISO}^{\;uu}}\right) \tag{3.21}$$

Further manipulation for Eq.((3.21)) yield:

$$f_{H_{SISO}^{uu}|H_{f\,SISO}^{\;uu}}\left(H_{SISO}^{uu}\middle|H_{f\,SISO}^{\;uu}\right)=\frac{\gamma_{SISO}^{2^{uu}}}{A_{0_{SISO}}^{\gamma^{2^{uu}}}H_{f\,SISO}^{\;uu}\;H_{a\,SISO}^{\;uu}}\left(\frac{H_{SISO}^{uu}}{H_{f\,SISO}^{\;uu}\;H_{a\,SISO}^{\;uu}}\right)^{\gamma_{SISO}^{2^{uu}}-1},$$

$$0\le H_{SISO}^{uu}\le A_{0_{SISO}}^{\;uu}H_{f\,SISO}^{\;uu}\;H_{a\,SISO}^{\;uu} \tag{3.22}$$

where $\gamma_{SISO}^{uu}=\frac{W_{zeq_{SISO}}^{uu}}{2\sigma_s}$. Substituting Eq.((3.22)) into Eq.((3.20)) gives:

$$f_{H_{SISO}^{uu}}\left(H_{SISO}^{uu};\mathrm{w}_{z_{SISO}}^{uu}\right)=\frac{\gamma_{SISO}^{2^{uu}}}{\left(A_{0_{SISO}}^{\;uu}H_{a\,SISO}^{\;uu}\right)^{\gamma^2}}H_{SISO}^{uu\;\gamma_{SISO}^{2^{uu}}-1}$$

$$\times\int_{\frac{H_{SISO}^{uu}}{A_{0_{SISO}}^{uu}H_{a_{SISO}}^{uu}}}^{\infty}H_{SISO}^{uu\;-\gamma_{SISO}^{2^{uu}}}f_{H_{f_{SISO}}^{uu}}\left(H_{f\,SISO}^{\;uu}\right)dH_{f\,SISO}^{\;uu} \tag{3.23}$$

By using lognormal distribution for weak turbulence, Eq.((3.23)) becomes:

$$f_{H_{SISO}^{uu}}\left(H_{SISO}^{uu}\right)=\frac{\gamma_{SISO}^{2^{uu}}}{\left(A_{0_{SISO}}^{\;uu}H_{a\,SISO}^{\;uu}\right)^{\gamma^2}}H_{SISO}^{uu\;\gamma_{SISO}^{2^{uu}}-1}$$

$$\times\int_{\frac{H_{SISO}^{uu}}{A_{0_{SISO}}^{uu}H_{a_{SISO}}^{uu}}}^{\infty}H_{SISO}^{uu\;-\gamma_{SISO}^{2^{uu}}}\frac{1}{2H_{f\,SISO}^{\;uu}\sqrt{2\pi\sigma_{x_{SISO}}^{2^{uu}}}}exp\left(\frac{\left(lnH_{f\,SISO}^{\;uu}+2\sigma_{x_{SISO}}^{2^{uu}}\right)}{8\sigma_{x_{SISO}}^{2^{uu}}}\right)dH_{f\,SISO}^{\;uu} \tag{3.24}$$

Simplifying and defining $\mu_{SISO}^{uu}=2\sigma_{x_{SISO}}^{2^{uu}}(1+2\gamma_{SISO}^{2^{uu}})$ results in:

$$f_{H_{SISO}^{uu}}\left(H_{SISO}^{uu};\mathrm{w}_{z_{SISO}}^{uu}\right)=\frac{\gamma_{SISO}^{2^{uu}}}{2\left(A_{0_{SISO}}^{\;uu}{}_{SISO}^{\;uu}H_{a\,SISO}^{\;uu}\right)^{\gamma_{SISO}^{2^{uu}}}}H_{SISO}^{uu\;\gamma_{SISO}^{2^{uu}}-1}$$

$$\times\,erfc\left(\frac{ln\left(\frac{H_{SISO}^{uu}}{A_{0_{SISO}}^{uu}H_{a_{SISO}}^{uu}}\right)+\mu_{SISO}^{uu}}{\sqrt{8}\sigma_{x_{SISO}}^{uu}}\right)e^{\left(2\sigma_{x_{SISO}}^{2^{uu}}\gamma_{SISO}^{2^{uu}}(1+\gamma_{SISO}^{2^{uu}})\right)} \tag{3.25}$$

where $\sigma_{x_{SISO}}^{2^{uu}}$ is the log amplitude variance for the UAV-UAV SISO-1 channel that its formulation depends on if the wave is a plane or spherical [54] as:

$$\sigma_{x_{SISO}}^{2^{uu}} = 0.30545\, K^{7/6}\, C_n^2(h) \mathrm{Z_{SISO}^{uu}}^{11/6} \approx \frac{\sigma_{R_{SISO}}^{2^{uu}}}{4} \qquad \text{For the plane wave} \tag{3.26}$$

$$\sigma_{x_{SISO}}^{2^{uu}} = 0.124\, K^{7/6}\, C_n^2(h) \mathrm{Z_{SISO}^{uu}}^{11/6} \qquad \text{For the spherical wave} \tag{3.27}$$

where $\sigma_{R_{SISO}}^{2^{uu}}$ is the Rytov variance for the UAV-UAV SISO-1 channel defined as:

$$\sigma_{R_{SISO}}^{2^{uu}} = 1.23\, C_n^2(h)\, K^{7/6}\, {Z_{SISO}^{uu}}^{11/6} \tag{3.28}$$

For simplicity, the parameters such as the link distance Z_{SISO}^{uu}, the transmitted power P_t, and the pointing error angle θ_r are taken equally for both the left and right arms between two adjustment drones.

3.2.2 UAV-GS SISO-2 Channel Modeling

The scenario of the UAV-GS SISO-2 channel is similar to the UAV-UAV SISO-1 channel but with varying at least one of the parameters stated in Eq.((3.1)). All the above equations containing Z and h in their formulation needed to be recalculated because this channel is dynamic. The received optical signal y_{SISO}^{uG} can be expressed as:

$$y_{SISO}^{uG} = H_{SISO}^{uG} xR + n \tag{3.29}$$

where H_{SISO}^{uG} is the channel gain of UAV-GS SISO-2 topology that can be expressed as:

$$H_{SISO}^{uG} = {H_a}_{SISO}^{uG}\, {H_f}_{SISO}^{uG}\, {H_p}_{SISO}^{uG} \tag{3.30}$$

where ${H_a}_{SISO}^{uG}$, ${H_f}_{SISO}^{uG}$, and ${H_p}_{SISO}^{uG}$ represent the attenuation result from the beam extinction due to absorption and scattering, scintillation impact, and geometric and pointing loss for the atmosphere channel, respectively, of the UAV-GS SISO-2 channel.

The attenuation $H_{a_{SISO}}^{uG}$ has been expressed by Beer-Lambert law $H_{a_{SISO}}^{uG} = exp(-Z_{SISO}^{uG}\sigma)$, where Z_{SISO}^{uG} is the path length between the GS and the main drone D_M. The atmospheric fading $H_{f_{SISO}}^{uG}$ can be expressed as:

$$H_{f_{SISO}}^{uG} = \frac{2Pr_{SISO}^{uG}}{\pi W_{SISO}^{uG}} \tag{3.31}$$

where $P_{r_{SISO}}^{uG}$ is the received power, and W_{SISO}^{uG} is beam spot radius at the receiver for the UAV-GS SISO-2. The pointing error $H_{p_{SISO}}^{uG}$ can be expressed as:

$$H_{p_{SISO}}^{uG} = A_{0_{SISO}}^{uG} \exp\left(\frac{-2r_{SISO}^{2^{uG}}}{W_{zeq_{SISO}}{}^{2^{uG}}}\right) \tag{3.32}$$

where $A_{0_{SISO}}^{uG} = \frac{2Z_{SISO}^{uG}}{Kw_0^2}$ is the fractional collected power at $Z_{SISO}^{uG}= 0$, r_{SISO}^{uG} is the radial displacement of the optical beam, and $W_{zeq_{SISO}}^{uG} = w_{z_{SISO}}^{2^{uG}} \frac{\sqrt{\pi}erf(v_{SISO}^{uG})}{2v\ exp(-v_{SISO}^{2^{uG}})}$ is the equivalent optical beam radius at the UAV-GS SISO-2 channel's receiver, $w_{z_{SISO}}^{uG}$ is the beam radius when the irradiance drops to e^{-2} of the axial value at a distance Z_{SISO}^{uG} and is associated with the beam waist w_0 as:

$$w_{z_{SISO}}^{uG} \approx w_0 \left[1 + \varepsilon_{SISO}^{uG}\left(\frac{\lambda Z_{SISO}^{uG}}{\pi w_0^2}\right)^2\right]^{\frac{1}{2}} \tag{3.33}$$

where $\varepsilon_{SISO}^{uG} = (1 + 2w_0^2/\rho_0^2(Z_{SISO}^{uG}))$, and the coherence length $\rho_0(Z_{SISO}^{uG}) = (0.55C_n^2(h)K^2Z_{SISO}^{uG})^{-3/5}$, and $v_{SISO}^{uG} = (\sqrt{\pi}\ a)/(\sqrt{2}\ w_{z_{SISO}}^{uG})$, where a is the receiver radius. The derivative of the PDF of H_{SISO}^{uG} by using lognormal distribution is flow the similar steps used in the UAV-UAV SISO-1 channel and is given as: $f_{H_{SISO}^{uG}}(H_{SISO}^{uG}; w_{z_{SISO}}^{uG}) = \frac{\gamma_{SISO}^{2^{uG}}}{2(A_{0_{SISO}}^{uG}H_{a_{SISO}}^{uG})^{\gamma^2}} H_{SISO}^{uG}{}^{\gamma_{SISO}^{2^{uG}}-1}$

$$\times erfc\left(\frac{ln\left(\frac{H^{uG}_{SISO}}{A_0{}^{uG}_{SISO}H_a{}^{uG}_{SISO}}\right)+\mu^{uG}_{SISO}}{\sqrt{8}\sigma^{uG}_{x_{SISO}}}\right)e^{\left(2\sigma^{2^{uG}}_{x_{SISO}}\gamma^{2^{uG}}_{SISO}(1+\gamma^{2^{uG}}_{SISO})\right)} \quad (3.34)$$

where $\gamma^{uG}_{SISO} = \frac{W^{uG}_{zeq_{SISO}}}{2\sigma_s}$, $\mu^{uG}_{SISO} = 2\sigma^{2^{uG}}_{x_{SISO}}(1 + 2\gamma^{2^{uG}}_{SISO})$, and $\sigma^{2^{uG}}_{x_{SISO}}$ is the UAV-GS SISO-2 channel's log amplitude variance of and can be expressed as:

$$\sigma^{2^{uG}}_{x_{SISO}} = 0.30545\, K^{7/6}\, C_n^2(h) \mathrm{Z}^{\mathrm{uG}}_{\mathrm{SISO}}{}^{11/6} \approx \frac{\sigma^{2^{uG}}_{R_{SISO}}}{4} \qquad \text{For plan wave} \quad (3.35)$$

$$\sigma^{2^{uG}}_{x_{SISO}} = 0.3124\, K^{7/6}\, C_n^2(h) \mathrm{Z}^{\mathrm{uG}}_{\mathrm{SISO}}{}^{11/6} \qquad \text{For spherical wave} \quad (3.36)$$

where $\sigma^{2^{uG}}_{R_{SISO}}$ is the Rytov variance that can be expressed to the SISO-2 channel as:

$$\sigma^{2^{uG}}_{R_{SISO}} = 1.23\, C_n^2(h) K^{7/6}\, Z^{uG}_{SISO}{}^{11/6} \quad (3.37)$$

3.2.3 UAVs-UAV MISO Channel Modeling

When the flow of the information is from the drones toward GS, the MISO topology is formed. The MISO configuration consists of many transmitting antennas that transmit the optical signals. Only one receiving antenna receives the optical signals from multiple transmitting antennas, which means numerous sources are available. However, there is only one destination available [55]. The link distance Z was assumed to be varied concerning changes in the altitude h or the link slop angle θ. The optical signal received at the receiver y_{MISO} expressed as:

$$y_{MISO} = xRH_{MISO} + v_n \quad (3.38)$$

where H_{MISO} is the channel gain of the MISO topology, and v_n is AWGN with variance $\sigma_n = N_0/2.0$ and zero mean. Each channel in the MISO topology is faded independently, and the channel state H_{MISO} can be found by:

$$H_{MISO} = \prod_{m=1}^{M} H_{a_m}\, H_{f_m} H_{p_m} \qquad m=1,2,3...M \quad (3.38)$$

where M is the MISO topology total channels, in another mean, the number of drones that are equal to two channels, one in each arm, H_{a_m}, H_{f_m}, and H_{p_m} represent the attenuation result from the beam extinction due to scattering and absorption, scintillation impact, and geometric and pointing loss of the MISO topology's mth channel. The attenuation H_{a_m} has been modeled by Beer-Lambert law as:

$$H_{a_m} = exp(-Z_m \sigma) \tag{3.39}$$

where Z_m is the link distance between the drone D_{11} or D_{21} and the drone D_M. The atmospheric fading H_{f_m} can be expressed as:

$$H_{f_m} = \frac{2P_{r_m}}{\pi W_m} \tag{3.40}$$

where P_{r_m} is the received power of the optical signal from mth drone, and W_m is the beam radius of the mth channel in the MISO topology. The pointing error H_{p_m} can be expressed as:

$$H_{p_m} = A_{0_m} \exp\left(\frac{-2r_m^2}{W_{Zeq_m}^2}\right) \tag{3.41}$$

where A_{0_m} is the fractional of the collected power at Z_m=0, $r_m = Z_m . \theta_{r_m}$ is the radial displacement, and $W_{Zeq_m} = w_{Z_m}^2 \frac{\sqrt{\pi} erf(v_m)}{2v\ exp(-v_m^2)}$ is the equivalent optical beam radius of the mth channel's receiver in MISO topology, $w_{Z_m}$is the beam radius at the distance Z_m where the irradiance drops to e^{-2} of the axial value and is associated with the beam waist w_0 as:

$$w_{Z_m} \approx w_0 \left[1 + \varepsilon_m \left(\frac{\lambda Z_m}{\pi w_0^2}\right)^2\right]^{\frac{1}{2}} \tag{3.42}$$

where $\varepsilon_m = (1 + 2w_0^2/\rho_0^2(Z_m))$, and the coherence length $\rho_0(Z_m) = (0.55C_n^2(h)K^2 Z_m)^{-3/5}$, and $v_m = (\sqrt{\pi}\ a) / (\sqrt{2}\ w_{Z_m})$, where a is the receiver radius.

The derivative of the PDF of the MISO channel gain H_m in weak atmospheric turbulence followed the same steps to the SISO channel except dividing the lognormal variance by the transmitting antenna number [56]. In the proposed system, the transmitting antennas are two. More than two is also possible if the drones sent their information directly to GS (not DF technique) or more than two arms in the proposed system. The PDF of the channel gain for the mth channel H_m can be expressed as:

$$f_{H_m}\left(H_m; w_{z_m}\right) = \frac{\gamma_m^2}{2\left(A_{0_m}\, H_{a_m}\right)^{\gamma^2}} {H_m}^{\gamma_m^2 - 1} \times erfc\left(\frac{ln\left(\frac{H_m}{A_{0m} H_m}\right) + \mu_m}{\sqrt{2}\sigma_{x_m}}\right) e^{\left(\sigma_{x_m}^2 \gamma_m^2 (1+\gamma_m^2)\right)}$$

(3.42)

The full PDF of the MISO topology is given as follows:

$$f_{MISO}^T = \sum_{m=1}^{M} f_{H_m}\left(H_m; w_{z_m}\right) \qquad m=1,2,3,\dots.M \tag{3.43}$$

where $\gamma_m = \frac{W_{Zeq_m}}{2\sigma_s}$, $\mu_m = \sigma_{x_m}^2(1 + 2\gamma_m^2)$, and $\sigma_{x_m}^2$ is the MISO channel log amplitude variance that is expressed for plane and spherical wave [54] after being modified to be suited the MISO channel as:

$$\sigma_{x_m}^2 = 0.30545\, K^{7/6}\, C_n^2(h) {Z_m}^{11/6} \approx \frac{\sigma_{R_m}^2}{4} \qquad \text{For plane-wave} \tag{3.44}$$

$$\sigma_{x_m}^2 = 0.124\, K^{7/6}\, C_n^2(h) {Z_m}^{11/6} \qquad \text{For spherical wave} \tag{3.45}$$

where $\sigma_{R_m}^2$ is the Rytov variance for the m^{th} MISO channel defined as:

$$\sigma_{R_m}^2 = 1.23\, C_n^2(h)\, K^{7/6}\, {Z_m}^{11/6} \tag{3.46}$$

For simplicity, all the parameter values for the two MISO topology channels have been assumed equal.

3.3 THE AVERAGE BIT ERROR (ABER)

The ABER results from multiplying the instantaneous conditional BER(H) by the channel gain H PDF and is expressed as [24]:

$$ABER = \int_0^\infty BER\ (H) \times f_H\ (H) dH \tag{3.47}$$

The instantaneous conditional BER(H) is the simulated conditional BER(H). The probability distribution integration solution of the lognormal is found [2] as:

$$f_H(H; w_z) = \frac{1}{2}\left[exp^{\gamma^2\Psi - 2\sigma_x^2\gamma^4} erfc\left(\frac{\Psi}{\sqrt{8}\sigma_x}\right) + erfc\left(\frac{4\sigma_x^2\gamma^2 - \Psi}{\sqrt{8}\sigma_x}\right)\right] \tag{3.48}$$

where $\Psi = ln\left(\frac{h_0}{A_0 H_a}\right) + u$, and $h_0 = \sqrt{C^{-1}(R_0)\sigma_n^2 / 2P_t^2 R^2}$, where C is the channel's capacity, which is the highest data rate that can be reliably sent between the transmitter and receiver, R_0 is the data rate, σ_n^2 is noise variance, P_t is a transmitted power, and R is a photodetector responsivity [2]. Substitute Eq.((3.48)) into Eq.((3.47)), the ABER becomes:

$$ABER = BER_{sim}(H) \times \frac{1}{2}\left[exp^{\gamma^2\Psi - 2\sigma_x^2\gamma^4} erfc\left(\frac{\Psi}{\sqrt{8}\sigma_x}\right) + erfc\left(\frac{4\sigma_x^2\gamma^2 - \Psi}{\sqrt{8}\sigma_x}\right)\right] \tag{3.49}$$

The ABER has been measured for each subsystem, and the TABER has been calculated.

3.3.1 ABER UAV-UAV SISO-1 Channels

The ABER of the UAV-UAV SISO channel can be expressed as:

$$ABER_{SISO}^{uu} = \int_0^\infty BER_{sim}\,(H_{SISO}^{uu}) \times f_{H_{SISO}^{uu}}\,(H_{SISO}^{uu}) dH_{SISO}^{uu} \tag{3.50}$$

where $BER_{sim}(H_{SISO}^{uu})$ is the simulated instantaneous BER conditioned on the UAV-UAV SISO-1 channel gain H_{SISO}^{uu}, and $f_{H_{SISO}^{uu}}\,(H_{SISO}^{uu})$ is the PDF of the UAV-UAV SISO-1 channel gain H_{SISO}^{uu} as expressed in Eq.(13). The solution to the integration of Eq.((3.25)) can be expressed as:

$$f_{H_{SISO}^{uu}}\left(H_{SISO}^{uu}; \mathrm{w}_{z_{SISO}}^{uu}\right) = \frac{1}{2}\begin{bmatrix} exp^{\gamma_{SISO}^{2^{uu}}\Psi_{SISO}^{uu} - 2\sigma_{x_{SISO}}^{2^{uu}}\gamma_{SISO}^{4^{uu}}} erfc\left(\frac{\Psi_{SISO}^{uu}}{\sqrt{8}\sigma_{x_{SISO}}^{uu}}\right) \\ +erfc\left(\frac{4\sigma_{x_{SISO}}^{2^{uu}}\gamma_{SISO}^{2^{uu}} - \Psi_{SISO}^{uu}}{\sqrt{8}\sigma_{x_{SISO}}^{2^{uu}}}\right) \end{bmatrix} \tag{3.51}$$

where $\Psi_{SISO}^{uu} = ln\left(\frac{h_0}{A_{0_{SISO}}^{uu} H_{a_{SISO}}^{uu}}\right) + u_{SISO}^{uu}$, substituted Eq.((3.51)) into Eq.((3.50)) yield:

$$ABER_{SISO}^{uu} = BER_{sim}\,(H_{SISO}^{uu}) \times \frac{1}{2}\begin{bmatrix} exp^{\gamma_{SISO}^{2^{uu}}\Psi_{SISO}^{uu} - 2\sigma_{x_{SISO}}^{2^{uu}}\gamma_{SISO}^{4^{uu}}} erfc\left(\frac{\Psi_{SISO}^{uu}}{\sqrt{8}\sigma_{x_{SISO}}^{uu}}\right) \\ +erfc\left(\frac{4\sigma_{x_{SISO}}^{2^{uu}}\gamma_{SISO}^{2^{uu}} - \Psi_{SISO}^{uu}}{\sqrt{8}\sigma_{x_{SISO}}^{2^{uu}}}\right) \end{bmatrix} \tag{3.52}$$

3.3.2 ABER UAV-GS SISO-2 Channel

The ABER of the UAV-GS SISO-2 channel can be expressed as:

$$ABER_{SISO}^{uG} = \int_0^{\infty} BER_{sim}\ (H_{SISO}^{uG}) \times f_{H_{SISO}^{uG}}\ (H_{SISO}^{uG})dH_{SISO}^{uG} \qquad (3.53)$$

where $BER_{sim}(H_{SISO}^{uG})$ is the simulated instantaneous BER conditioned on the UAV-GS SISO-2 channel gain H_{SISO}^{uG}, and $f_{H_{SISO}^{uG}}\ (H_{SISO}^{uG})$ is the PDF of the UAV-GS SISO-2 channel gain H_{SISO}^{uG} as expressed in Eq.((19)). The solution to the integration of Eq.((3.33)) can be expressed as:

$$f_{H_{SISO}^{uG}}\left(H_{SISO}^{uG}; \mathrm{w}_{z_{SISO}}^{uG}\right) = \frac{1}{2}\begin{bmatrix} exp^{\gamma_{SISO}^{2uG}\Psi_{SISO}^{uG} - 2\sigma_{x_{SISO}}^{2uG}\gamma_{SISO}^{4uG}} erfc\left(\frac{\Psi_{SISO}^{uG}}{\sqrt{8}\sigma_{x_{SISO}}^{uG}}\right) \\ + erfc\left(\frac{4\sigma_{x_{SISO}}^{2uG}\gamma_{SISO}^{2uG} - \Psi_{SISO}^{uG}}{\sqrt{8}\sigma_{x_{SISO}}^{2uG}}\right)\end{bmatrix} \qquad (3.54)$$

where $\Psi_{SISO}^{uG} = ln\left(\frac{h_0}{A_{0_{SISO}}^{uG} H_{a_{SISO}}^{uG}}\right) + u_{SISO}^{uG}$, substituted Eq.((3.54)) into Eq.((3.53)) yield:

$$ABER_{SISO}^{uG} = BER_{sim}\ (H_{SISO}^{uG}) \times \frac{1}{2}\begin{bmatrix} exp^{\gamma_{SISO}^{2uG}\Psi_{SISO}^{uG} - 2\sigma_{x_{SISO}}^{2uG}\gamma_{SISO}^{4uG}} erfc\left(\frac{\Psi_{SISO}^{uG}}{\sqrt{8}\sigma_{x_{SISO}}^{uG}}\right) \\ + erfc\left(\frac{4\sigma_{x_{SISO}}^{2uG}\gamma^{2} - \Psi_{SISO}^{uG}}{\sqrt{8}\sigma_{x_{SISO}}^{2uG}}\right)\end{bmatrix} \qquad (3.55)$$

3.3.3 ABER UAV-UAV MISO Channel

The ABER of the m^th channel in the MISO channel can be expressed as:

$$ABER_m = \int_0^{\infty} BER_{sim}\ (H_m) \times f_{H_m}\ (H_m)dH_m \qquad m=1,2,3,\ldots M \qquad (3.56)$$

where $BER_{sim}(H_m)$ is the simulated instantaneous BER conditioned on the m^th channel gain H_m of the MISO topology. The solution of the integration of the PDF of the Eq.((3.42)) of the m^th channel gain H_m can be expressed as:

$$f_{H_m}\left(H_m; w_{z_m}\right) = \frac{1}{2}\left[exp^{\gamma_m^2\Psi_m - \sigma_{x_m}^2\gamma_m^4} \times erfc\left(\frac{\Psi_m}{\sqrt{2}\sigma_{x_m}}\right) + erfc\left(\frac{2\sigma_{x_m}^2\gamma_m^2 - \Psi_m}{\sqrt{2}\sigma_{x_m}^2}\right)\right] \qquad (3.57)$$

where $\Psi_m = ln\left(\frac{h_0}{A_{0_m} H_{a_m}}\right) + \mu_m$, substituted Eq.((3.57)) into Eq.((3.56)) yields:

$$ABER_m = BER_{sim}\ (H_m) \times \frac{1}{2}\left[exp^{\gamma_m^2 \Psi_m - \sigma_{x_m}^2 \gamma_m^4} erfc\left(\frac{\Psi_m}{\sqrt{2}\sigma_{x_m}}\right) + erfc\left(\frac{2\sigma_{x_m}^2 \gamma_m^2 - \Psi_m}{\sqrt{2}\sigma_{x_m}^2}\right)\right] \quad (3.58)$$

Then, the total ABER of the MISO topology can be expressed as:

$$ABER_{MISO} = 1 - \prod_{m=1}^{M}(1 - ABER_m) \qquad m=1,2,3,\ldots.M \qquad (3.59)$$

The overall system ABER that includes the ABER of the SISO-1, SISO-2, and MISO channels can be calculated as [43]:

$$TABER = 1 - \prod_{l=1}^{N}(1 - ABER_l) \qquad l=1,2,3,.N \qquad (3.60)$$

where l is the l^{th} channel, N is the total drones equal to the total channels in the system, and $ABER_l$ refers to the average bit error rate for each channel.

4. THE RESULTS AND DISCUSSION

4.1 INTRODUCTION

The obtained results are from the mathematical expressions mentioned in the previous section. The results showed the capability to implement the flying system with pointing error factor H_p. The gotten performance in terms of ABER $\approx 10^{-8}$. The system was formed using two SISO topologies and one MISO topology. As shown in Figure 3.1, the drone's swarm moves away from the GS. The link distance Z between the GS and the flying system will increase; these increases occur due to increasing the system altitude h and constant zenith angle θ of the link or decreasing the zenith angle θ at fixed system altitude h. On the other hand, when the drones swarm flow toward the GS, the link distances Z between the GS and the flying system reduces in two cases, reducing Z due to changing the altitude h and the zenith angle θ or changing θ at a fixed h. The first scenario was adopted to determine when the system failed at a specific pointing error angle θ_r and link distance Z. The results were divided into three parts, as shown in Figure 4.1.

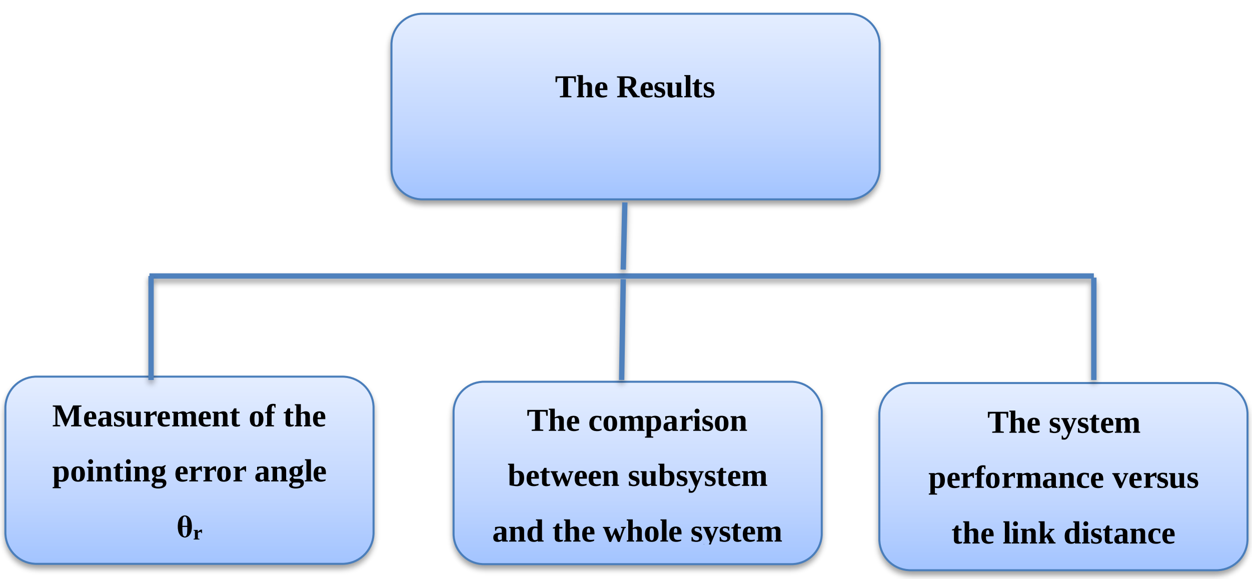

Figure 4.1: The thesis results

The first part shows the pointing error angles θ_r values and the valuable link distances Z at different receiver diameters D_R range from 1 cm to 10 cm to maintain high system performance. The second part shows the comparison between the subsystems and the overall system. Finally, the third part treats the flying system as one drone and examines the maximum link distance Z that the system can reach.

4.2 MEASUREMENT OF THE POINTING ERROR ANGLE

In this section, the pointing error angles θ_r were measured at a specified link distance Z using different receiver diameters D_R. These measurements aimed to specify the pointing error angles θ_r that get high system performance and extract which one leads the system to fail. The parameters used in the tests as shown in Table 4.1. The first test examines the limited distance Z for the pointing error angles $\theta_r = 10^{-3}$, 10^{-4}, and 10^{-5} rad when the receiver diameter D_R =1 cm, and the results as shown in Figure 4.2. The pointing error angle θ_r of the optical beam between the drones in an arm of the V-shape was selected to be $1 \times 10^{-4}, 1 \times 10^{-5}$ rad because the distance Z_d = 60 m is not affected even if select $\theta_r = 10^{-3}$ rad. Through several trial-and-error experiments to determine the distance of the link, we found that the system got high BER at the pointing error angle $\theta_r = 10^{-3}$ rad and the link distance Z =1050 m. Therefore, $\theta_r = 10^{-3}$ rad at Z =1050 m and D_R = 1 cm can not be applied.

Table 4.1: The whole system and subsystem parameters.

Parameter	Symbol	Value
Distance between the GS and D_M	Z	Varying
Distance between the drones in the same arm	Z_d	60 m
Altitude	h	1000 m
Receiver Diameter	D_R	1 cm~10 cm
Pointing Error Angle between the GS and D_M	θ_r	$1 \times 10^{-3}, 1 \times 10^{-4}, 1 \times 10^{-5}$ rad
Pointing Error Angle between two drones	θ_{rd}	$1 \times 10^{-4}, 1 \times 10^{-5}$ rad

The altitude h of the flying system for the pointing error angle $\theta_r = 10^{-3}$ rad can exceed 1000 m when the flying system becomes perpendicular to the GS (Z=h). The recommended pointing angle $\theta_r < 10^{-4}$ rad for long-distance application (inter-satellite laser communication), where the receiver diameter D_R was fixed to 250 cm [5].

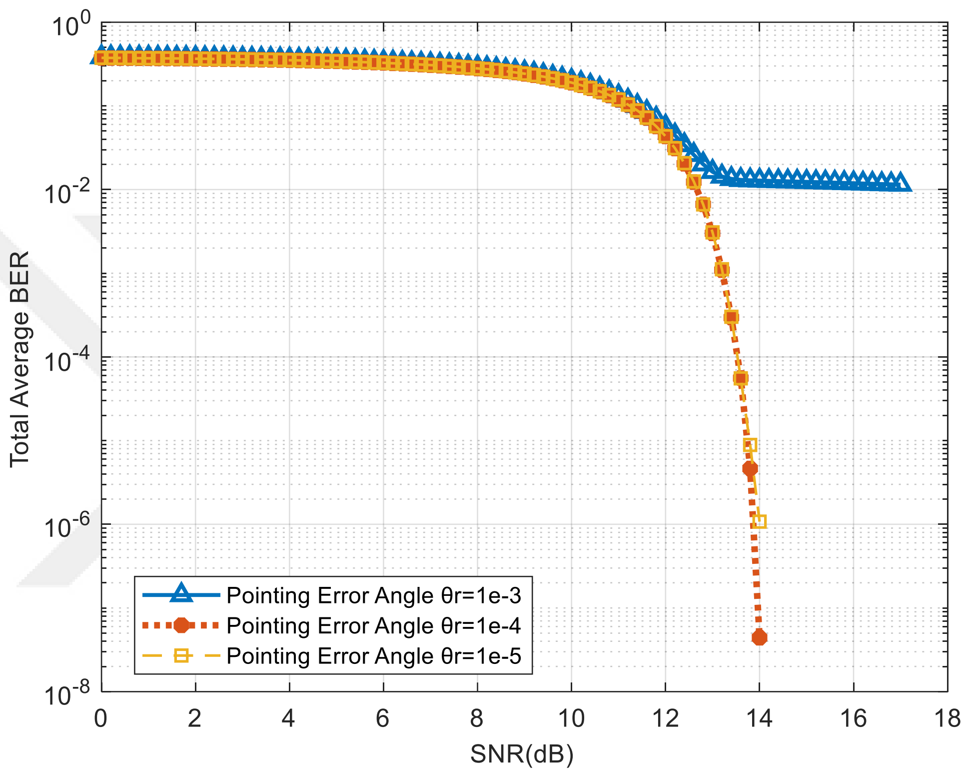

Figure 4.2: The system performance at $\theta_r = 10^{-3}, 10^{-4}, 10^{-5}$rad, Z=1050 m, and D_R= 1 cm.

At the same system parameters mentioned in the first test, except for the receiver diameter D_R=10 cm, the system did not get high BER at $\theta_r = 10^{-3}$ rad as shown in Figure 4.3. The increase in receiver diameter D_R means the increase in the received optical power captured by the receiver. Optically, as the distance a beam must travel from the transmitter to the receiver increases, the angular width of the beams expands, and the receiver may not be covered entirely, resulting in optical power loss. Therefore, selecting the pointing error angle θ_r value must jointly select the receiver diameter D_R.

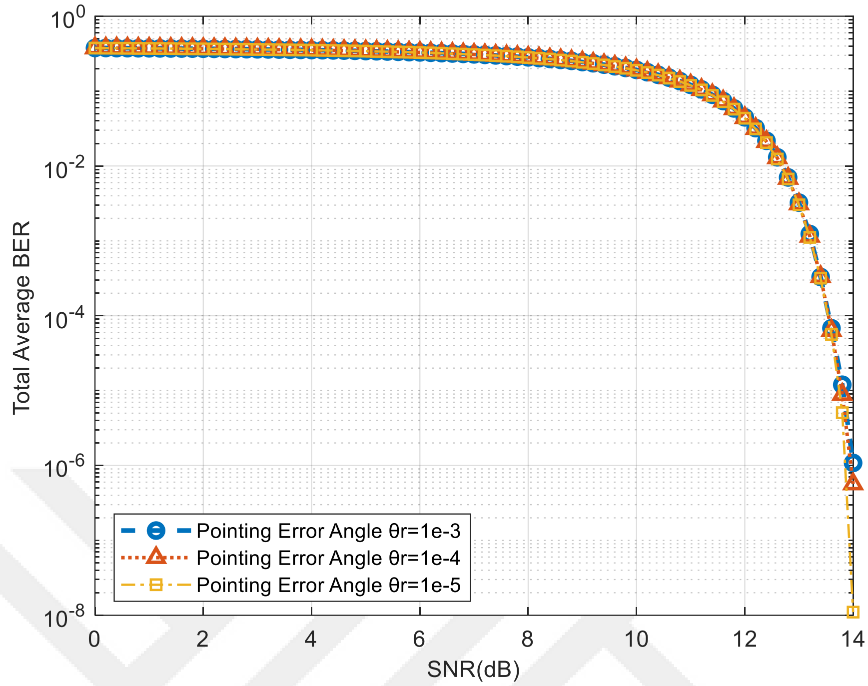

Figure 4.3: The system performance at $\theta_r = 10^{-3}, 10^{-4}, 10^{-5}$ rad, Z=1050 m, and D_R= 10 cm.

The second test was to examine the limited link distance Z for the pointing error angles $\theta_r = 10^{-4}$ and 10^{-5} rad at the receiver diameter D_R = 1 cm. Through several trial-and-error experiments and by gradually increasing the link distance Z value to determine the distance of the link. The result showed that Z's maximum link distance could reach 7500 m with TABER$\approx 10^{-8}$ for both angles, as shown in Figure 4.4. The increase in the link distance Z allowed the flying system coverage more area, but at the cost of performance, where the TABER=10^{-2} for the pointing error angle $\theta_r = 10^{-4}$ rad, and the TABER=10^{-7} for the pointing error angle θ_r =10^{-5} rad, as shown in Figure 4.5. The high TABER for the pointing error angle $\theta_r = 10^{-4}$ rad is due to the radial displacement r of the optical beam becoming high; consequently, the receiver catches part of the light beam, and the remaining beam is lost. At link distance Z=9800 m, both pointing error angles $\theta_r = 10^{-4}$ and 10^{-5} rad showed high TABER, as shown in Figure 4.6. Therefore, for short length applications such as drone systems, the range of link distance Z is between 7500~8800 m for the pointing error angle $\theta_r = 10^{-4}$ rad, and between 7500 and <9800 m for the pointing error angle $\theta_r = 10^{-5}$ rad.

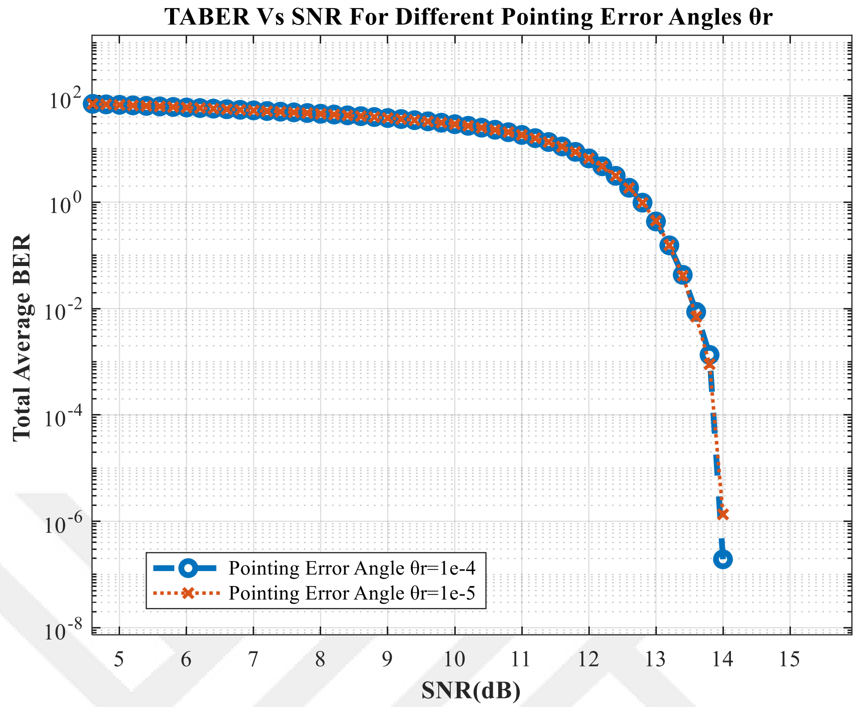

Figure 4.4: The system performance at $\theta_r = 10^{-4}, 10^{-5}$ rad, *Z*=7500 m, and D_R= 1 cm.

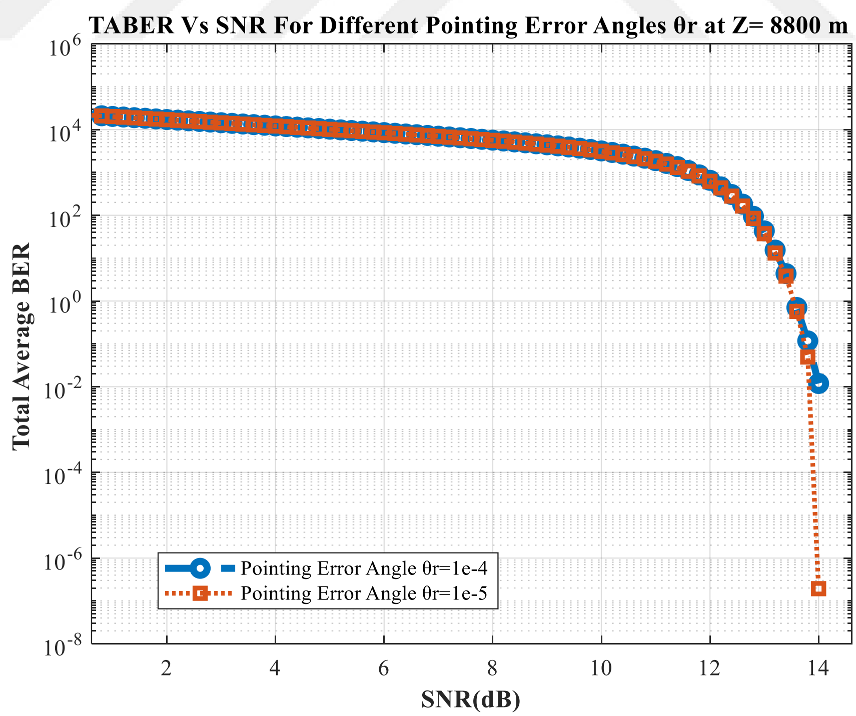

Figure 4.5: The system performance at $\theta_r = 10^{-4}, 10^{-5}$ rad, *Z*=8800 m, and D_R= 1 cm.

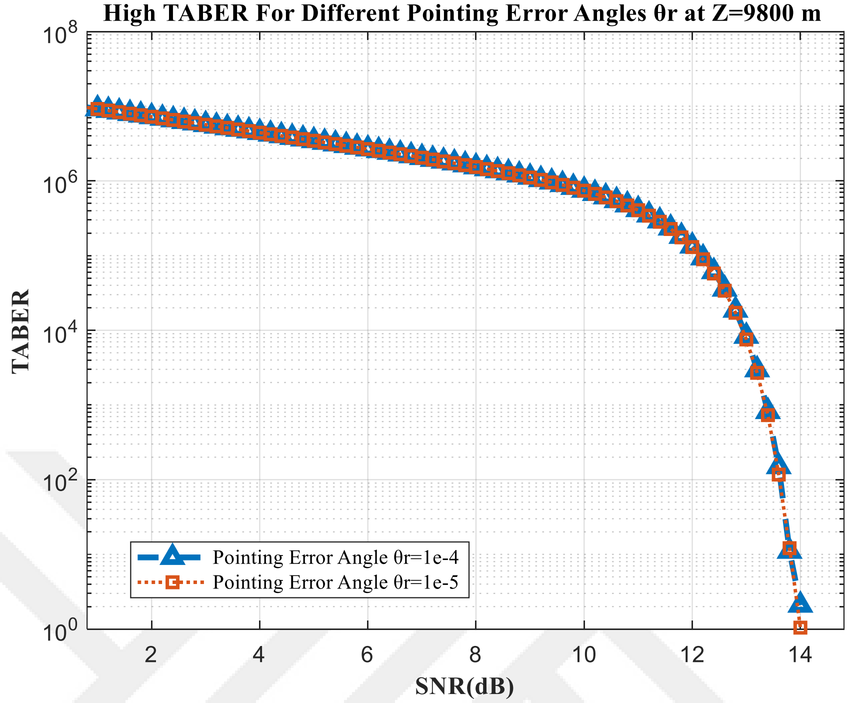

Figure 4.6: The system performance at $\theta_r = 10^{-4}, 10^{-5}$ rad, Z=9800 m, and D_R= 1 cm

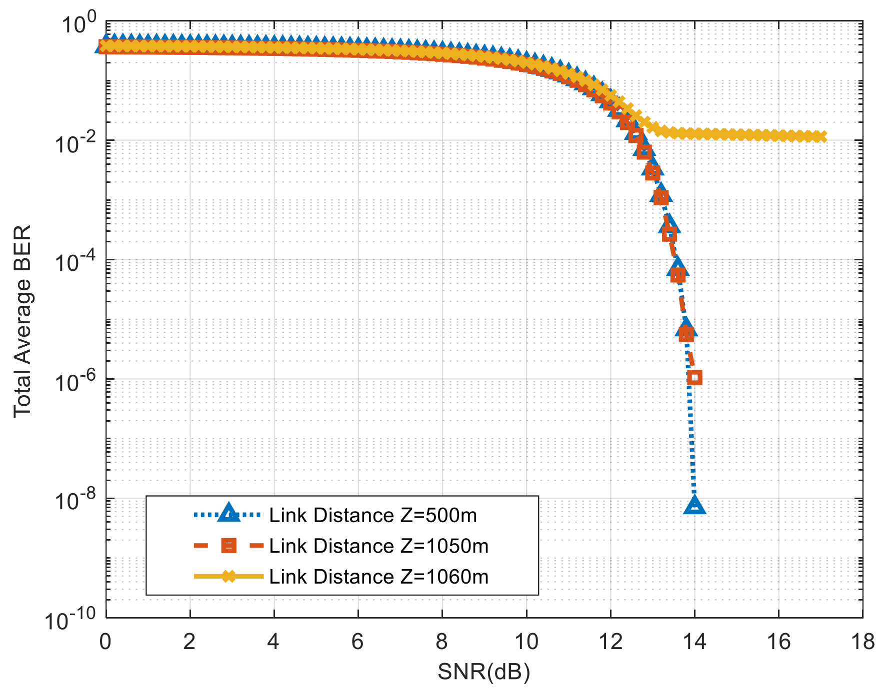

Figure 4.7: The system performance at $\theta_r = 10^{-3}$ rad, Z=1060 m, and D_R= 2 cm.

The subsequent tests will focus on the limited link distances Z for the pointing error angles $\theta_r = 10^{-3}$ rad when increasing the receiver diameter D_R more than 1 cm. For D_R=2 cm, through several trial-and-error experiments to determine the distance of the link, we found that the limited link distance Z is 1059 m, as shown in Figure 4.7. The system got high BER at Z=1060 m. The link distance Z increased 10 m when the receiver diameter D_R one centimeter increased compared to the previous Figure 4.2.

For the receiver diameter D_R=3 cm, and through several trial-and-error experiments to determine the distance of the link, we found that the system got high BER at Z=1087 m, as shown in Figure 4.8. Therefore, for pointing error angle $\theta_r = 10^{-3}$ rad and receiver diameter D_R=3 cm, the limited link distance Z=1086 m. The link distance Z increased 27 m when the receiver diameter D_R one centimeter increased compared to the previous Figure 4.7.

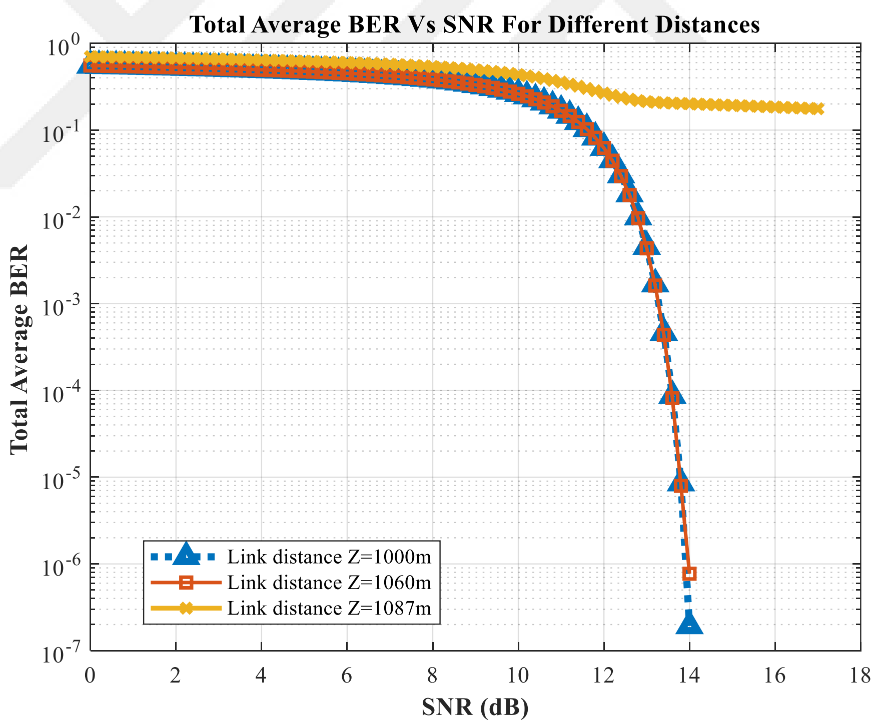

Figure 4.8: The system performance at $\theta_r = 10^{-3}$ rad, Z=1087 m, and D_R= 3 cm.

Further, increase the receiver diameter to become D_R=4 cm. Through several trial-and-error experiments to determine the distance of the link, we found that the system got high BER at Z=

1130 m, as shown in Figure 4.9. The link distance Z increased 43 m when the receiver diameter D_R one centimeter increased compared to the previous Figure 4.7.

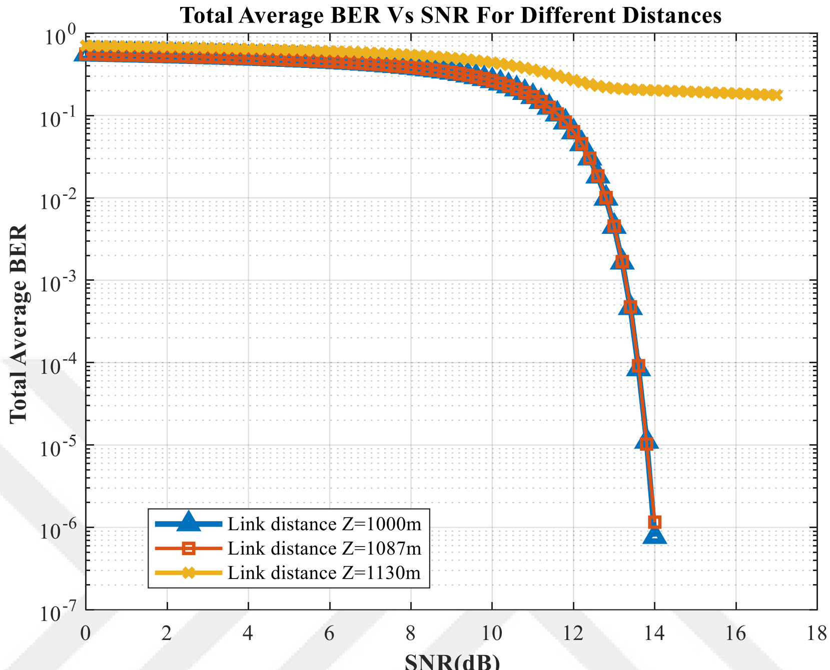

Figure 4.9: The system performance at $\theta_r = 10^{-3}$ rad, Z=1130 m, and D_R= 4 cm.

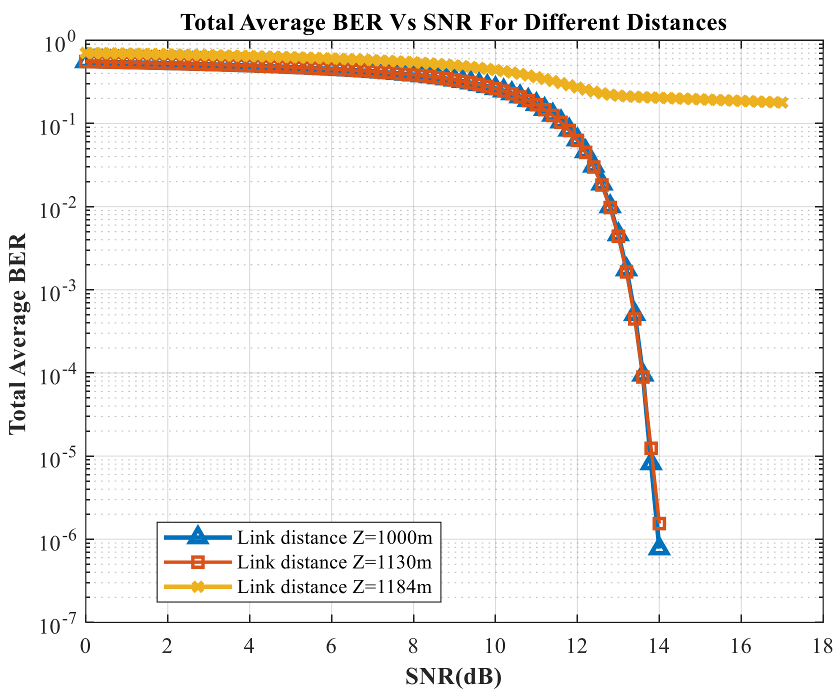

Figure 4.10: The system performance at $\theta_r = 10^{-3}$ rad, Z=1184 m, and D_R= 5 cm.

For the receiver diameter D_R=5 cm, and through several trial-and-error experiments to determine the distance of the link, we found that the system got high BER at Z= 1184 m, as shown in Figure 4.10. The link distance Z increased 54 m when the receiver diameter D_R one centimeter increased compared to the previous Figure 4.9.

The results of increased receiver diameter D_R from 6 cm to 10 cm, in addition to the results from 1 cm to 5 cm, as shown in the figures above, were summarized in Table 4.2. The beamwidth radius w_z in Table 4.2 increased as the link distance Z increased, enabling the receiver to capture more optical power and increase the system performance.

Table 4.2: The results of system performance at $\theta_r = 10^{-3}$ rad.

The Receiver Diameter D_R (cm)	The applicable distance Z (m)	The system failed (m)	The system altitude h (m)	Beam Waist Wz (cm)
1	1~1049	1050	1~ < 1050	5.44
2	1~1059	1060	1~ < 1060	5.45
3	1~1086	1087	1~ < 1087	5.47
4	1~1129	1130	1~ < 1130	5.51
5	1~1183	1184	1~ < 1184	5.56
6	1~1254	1255	1~ < 1255	5.63
7	1~1341	1342	1~ < 1342	5.72
8	1~1444	1445	1~ < 1445	5.85
9	1~1565	1566	1~ < 1566	6
10	1~1702	1703	1~ < 1703	6.19

Now move to extract the limited link distances Z that can be applied for the pointing error angle $\theta_r = 10^{-2}$ rad. The first test was at the receiver diameter D_R=1 cm. Figure 4.11 showed that through several trial-and-error experiments to determine the link's distance, and we found that the system's high BER is at $Z \leq 97$ m. The increases in the receiver diameter D_R=2 cm correspond to increases in the range of link distances Z at the same pointing error $\theta_r = 10^{-2}$rad.

As shown in Figure 4.12, the system's high BER at $Z \leq 99$ m. The increase in the link distance Z equaled 3 m when the receiver diameter increased by one centimeter compared to Figure 4.11.

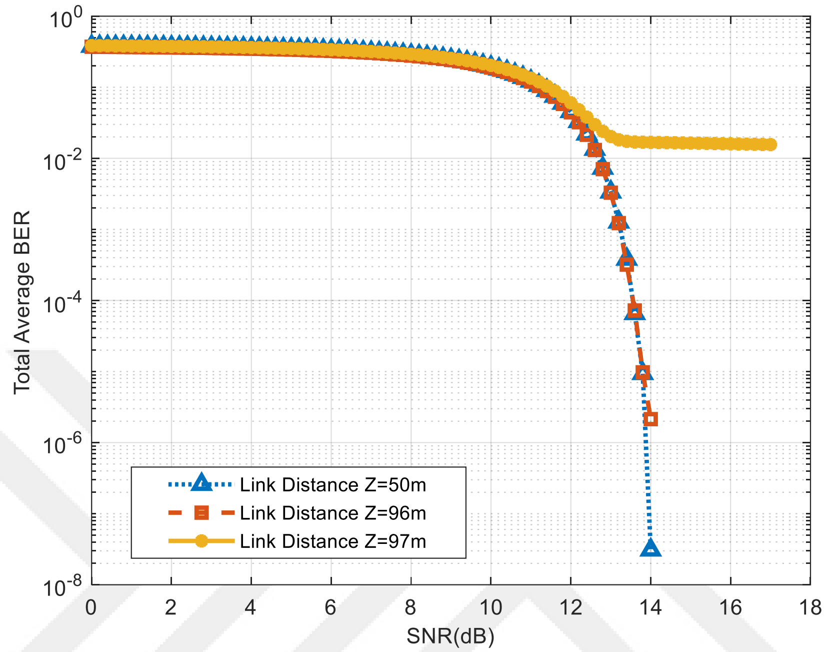

Figure 4.11: The system performance at $\theta_r = 10^{-2}$rad, Z=97 m, and D_R= 1 cm.

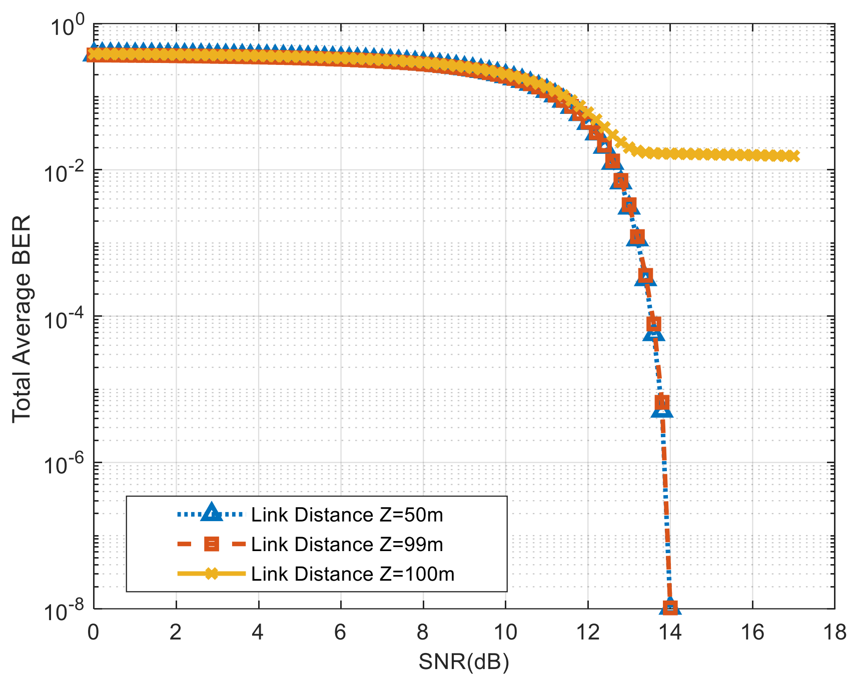

Figure 4.12: The system performance at $\theta_r = 10^{-2}$rad, Z=100 m, and D_R= 2 cm.

At the receiver diameter D_R=3 cm, and through several trial-and-error experiments to determine the distance of the link, we found that the system's high BER is at $Z \leq 101$ m, as shown in Figure 4.13, one meter more than the result in Figure 4.12.

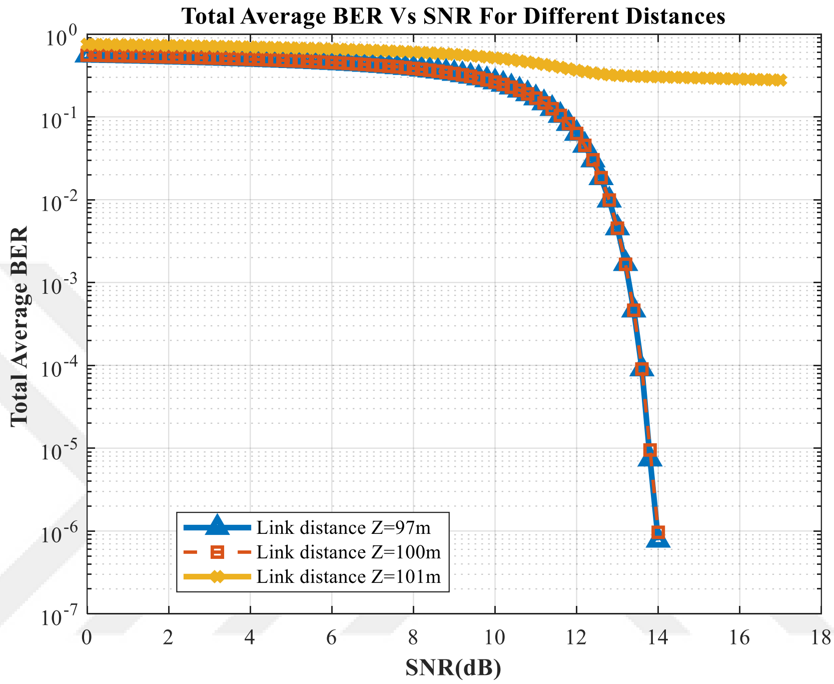

Figure 4.13: The system performance at $\theta_r = 10^{-2}$rad, Z=101 m, and D_R= 3 cm.

At the receiver diameter D_R=4 cm, and through several trial-and-error experiments to determine the distance of the link, we found that the system's high BER is at $Z \leq 105$ m, as shown in Figure 4.14, four meters the link distance *Z* increased compared to the result in Figure 4.13.

While at the receiver diameter D_R=5 cm, and through several trial-and-error experiments to determine the distance of the link, we found that the system's high BER is at $Z \leq 101$ m, as shown in Figure 4.15, five meters the link distance *Z* increased compared to the result in Figure 4.14.

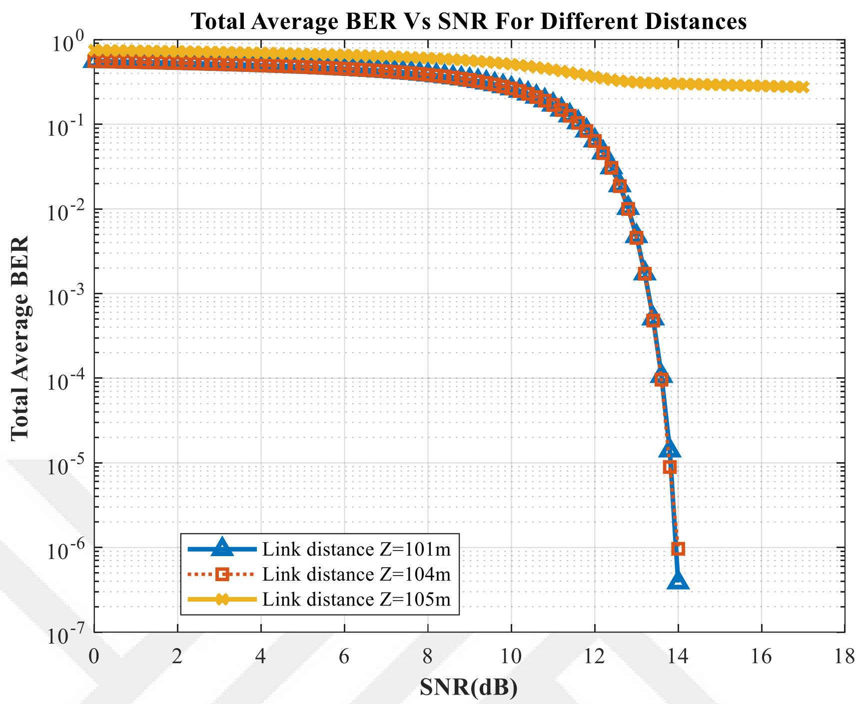

Figure 4.14: The system performance at $\theta_r = 10^{-2}$rad, Z=105 m, and D_R= 4 cm.

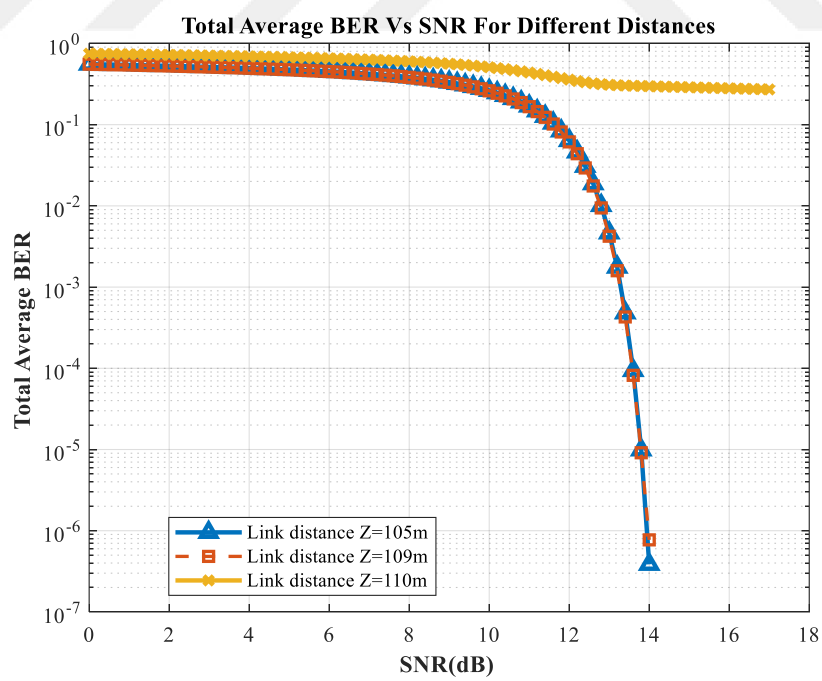

Figure 4.15: The system performance at $\theta_r = 10^{-2}$rad, Z=110 m, and D_R= 5 cm.

The rest of the tests for the pointing error angle $\theta_r = 10^{-2}$ rad and the receiver diameter range from 6~10 cm, in addition to the previous test results shown in the figures above, were summarized in Table 4.3, which showed a different range of link distances.

Table 4.3: The results at $\theta_r = 10^{-2}$ rad.

The Receiver Diameter D_R (cm)	The applicable distance *Z* (m)	The system failed (m)	The system altitude *h* (m)	Beam Waist *Wz* (cm)
1	1~96	97	1~ < 97	5
2	1~99	100	1~ < 100	5
3	1~100	101	1~ < 101	5
4	1~104	105	1~ < 105	5
5	1~109	110	1~ < 110	5
6	1~116	117	1~ < 117	5.01
7	1~126	127	1~ < 127	5.01
8	1~136	137	1~ < 144	5.01
9	1~151	152	1~ < 152	5.01
10	1~169	170	1~ < 170	5.01

Further increases in the pointing error angle $\theta_r = 10^{-1}$ rad will decrease the limited link distance Z that can be applied in the flying system even if increase the receiver diameter D_R. Figure 4.16 demonstrated that for the pointing error angle $\theta_r = 10^{-1}$ rad and the receiver diameter D_R=1 cm, the limited link distance Z=10 m. While the receiver diameter D_R=10 cm, the limited link distance Z=17 m, as shown in Figure 4.17.

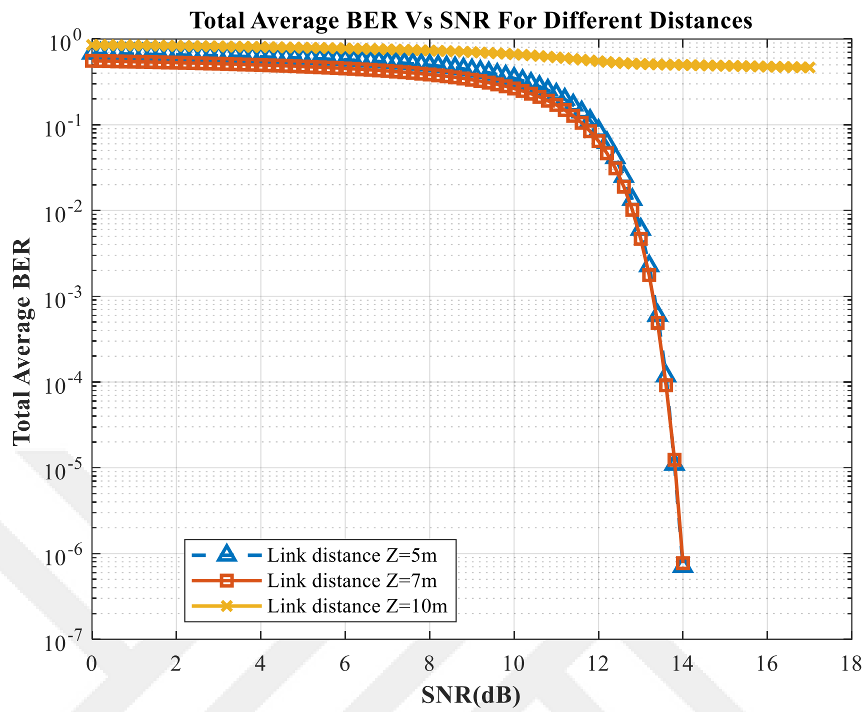

Figure 4.16: The system performance at $\theta_r = 10^{-1}$rad, Z=10 m, and D_R= 1 cm.

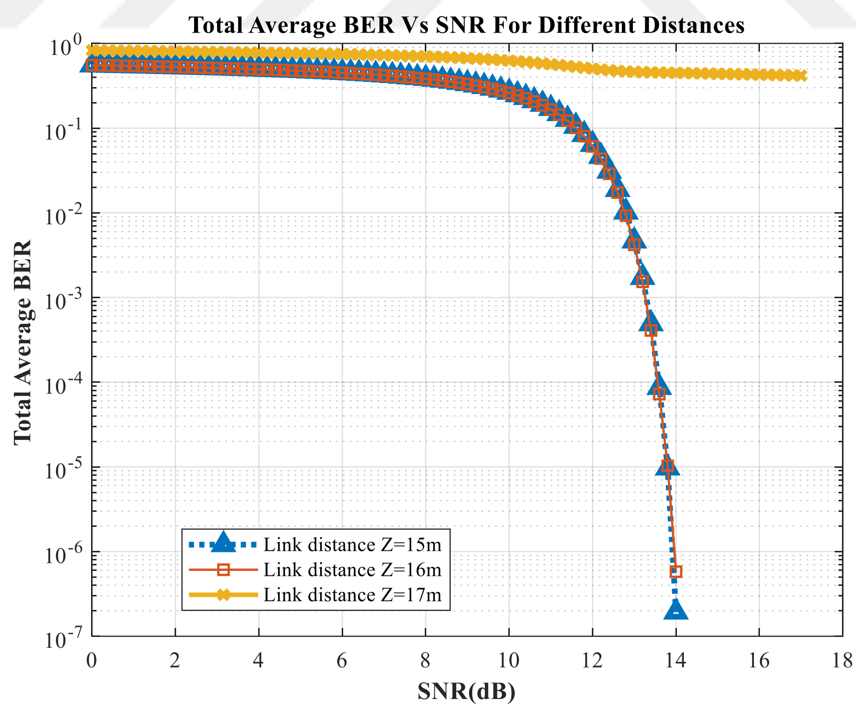

Figure 4.17: The system performance at $\theta_r = 10^{-1}$ rad, Z=17 m, and D_R= 10 cm.

4.3 THE SYSTEM PERFORMANCE

In this section, the purpose is to compare the performance of the subsystems measured in terms of ABER and the performance of the overall system measured in TABER, as shown in Figure 4.18. The parameters used in this test are shown in Table 4.4.

Table 4.4: The whole system and subsystem parameters.

Parameter	Symbol	Value
Distance between the GS and D_M	*Z	1000 m
Distance between the drones in the same arm	Z_d	60 m
Altitude	h	1000 m
Receiver Diameter	D_R	1 cm, and 10 cm
Pointing Error Angle between the GS and D_M	θ_r	1×10^{-5} rad
Pointing Error Angle between two drones	θ_{rd}	1×10^{-5} rad

*The link distance Z can be range from 1000 m to the limited value for the pointing error angle $\theta_r = 10^{-5}$ rad as measured in the previous section.

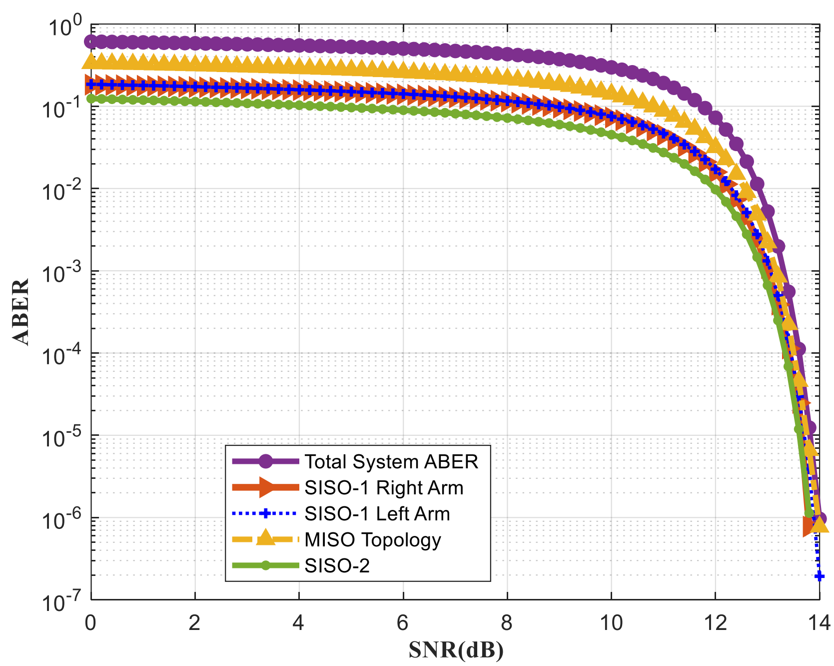

Figure 4.18: Performance comparison between the subsystems and the overall system.

In Figure 4.16, each part and the overall system showed lower performance at SNR $<$ 10 dB. After SNR $\geq$ 10 dB, there was an improvement in the performance gradually. At SNR $\geq$ 12 dB, the enhancement in the performance was evident from 10^{-2} to$\approx 10^{-8}$. Furthermore, there was no enhancement in the performance when increasing the receiver aperture diameter D_R from 1 cm to 10 cm.

When setting the ABER=10^{-4} as a reference value, the differences in SNR for each subsystem and the overall system are shown in Figure 4.19.

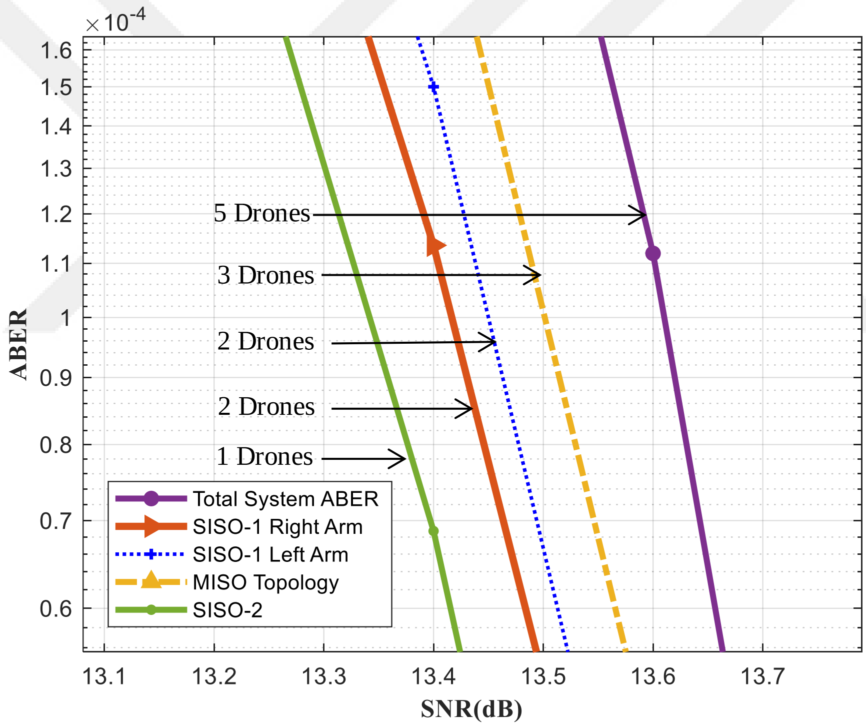

Figure 4.19: The SNR differences between the subsystem and the overall system at D_R=1 cm.

From Figure 4.19, the difference in SNR values for each part of the flying system and the whole system, as shown in Table 4.5, clarified that the SNR values increased as the number of drones increased. Thus, for example, in the whole system with five drones, the SNR=13.62 dB, while for the SISO-2 subsystem with one drone, the SNR=13.349 dB, and the difference between them is 0.271 dB.

Table 4.5: The differences in SNR for the whole system and the subsystems

System Part	Number of Drones	SNR(dB)
The whole system	5	13.62
MISO topology	3	13.50
SISO-1 left arm	2	13.45
SISO-1 right arm	2	13.425
SISO-2	1	13.349

4.4 THE SYSTEM PERFORMANCE VERSUS LINK DISTANCE

In this section, the five drones were considered a single system connected by an optical link with the GS. The purpose is to examine the system performance as the link distance Z increase bigger than 1000 m. For example, link distances Z = 2000, 6000, and 8500 m as samples. We take the total average BER (TABER) of the whole system in this case. The parameters used in this test as shown in Table 4.6. The flying system is perpendicular to the GS when the altitude h equals the link distance Z. When $Z > h$, it means a decrease in zenith angle θ, and the flying system moves away from the GS. The result of the three distances is shown in Figure 4.20.

Table 4.6: The whole system parameters.

Parameter	Symbol	Value
Distance between the GS and the system	Z	1000, 6000, 8500m
Altitude	h	1~1000m
Receiver Diameter	D_R	1 cm~10 cm
Pointing Error Angle	θ_r	$\leq 1 \times 10^{-4}$ rad

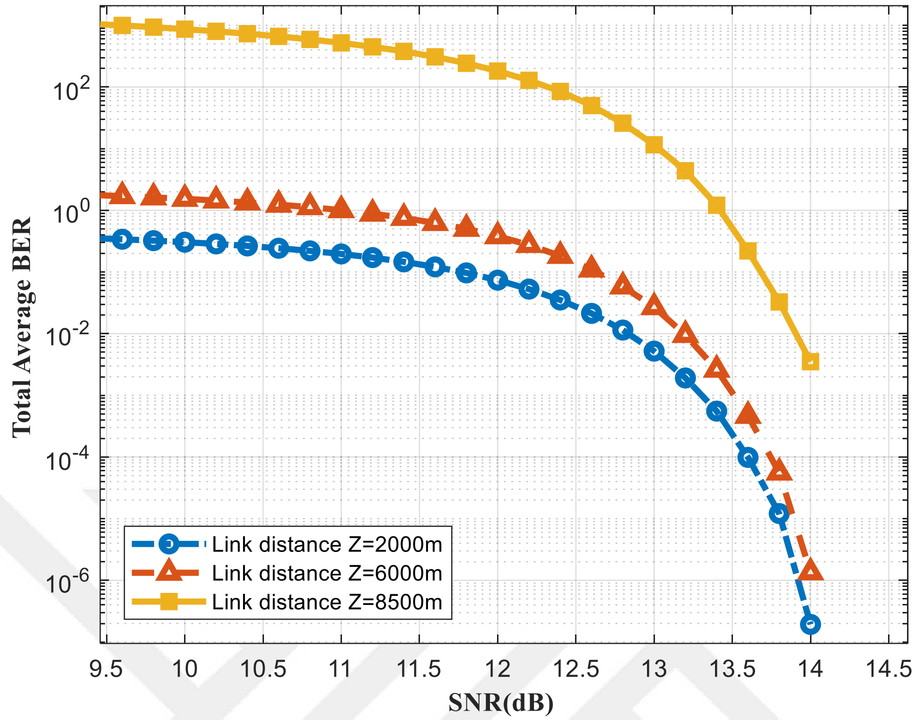

Figure 4.20: System performance for different link distances Z at D_R=1 cm.

At SNR$<$ 10 dB, all the distances showed the worst performance. After SNR$\geq$ 10 dB, there was an enhancement in the performance until TABER $\approx$ 10^{-7} for distances Z= 2000 and 6000 m. When Z increase, the system performance decreases, and vice versa. Table 4.7 summarized the results for increases in the link distances Z at TABER10^{-4}.

Table 4.7: The system performance when the link distance Z increases at D_R=1 cm.

The link distance Z(m)	**SNR(dB)**	**The radial displacement (r) rad**	**w_z(m)**	**H_p**
2000	13.601	0.0200	0.0668	0.0093
6000	13.75	0.0600	0.2885	5.5075×10^{-4}
8500	-	0.0850	0.7273	9.1967×10^{-5}

At Z=8500 m, the system showed the worst performance; therefore, at the values of the given parameter, Z must be $<$ 8500 m. The worst performance occurs when the link distance Z

increases, increasing the radial displacement r; therefore, the pointing error factor H_p decreases; consequently, the channel gain H decreases. Furthermore, there was no enhancement in the system's performance for the three-link distances when increasing the receiver aperture diameter D_R from 1 cm to 10 cm.

5. THE CONCLUSIONS

5.1 INTRODUCTION

This dissertation's system configuration depended on the previous design used in the study by Wamidh et al. [43]. The parameters selected carefully, such as the transmitted power P_t not low or high, low attenuation wavelength λ, the altitude h does not exceed the link distance Z value, and the receiver diameter D_R commensurate with the drone's applications.

The V-shape system consists of two topologies: MISO and SISO topologies, and each topology can be considered an independent system. Therefore, there were three subsystems in one system; two SISO topologies, each with different parameters, and one MISO topology with different parameters and requirements from the SISO topologies. These topologies were connected optically to form the whole system.

The system flew in a weak atmospheric turbulence regime and exposed channel gain H. The channel gain H was considered to consist of three factors. The most crucial factor is the pointing error H_p. The pointing error H_p consists of significant sub-parameters: the pointing error angle θ_r of the optical beam, the link distance Z, and the beamwidth w_z. There is a limitation for using the pointing error angle θ_r [5] that recommends the pointing error angle θ_r must be $< 10^{-4}$ rad for long link distances Z. The increase in the link distance Z makes the beam broader. The receiver catches part of the incident optical; therefore, the radial displacement r ($r \propto \theta_r$) must be as small as possible.

The purposes of the tests were to extract the values of the pointing error angles θ_r that are $> 10^{-4}$ rad at a particular link distance Z enables the designer to implement it in the short link applications such as the proposed system in this dissertation. The results can be helpful for the human controller to adjust and modify the link distances between drones.

The results of the tests were summarized in the following points:

a. Increasing the pointing error angle θ_r is not recommended, so the LOS between the transmitter and receiver is not precise.

b. The increase in the pointing error angle θ_r must correspond decrease in the link distances Z.

c. When there is a necessity to simultaneously increase the pointing error angle θ_r and the link distance Z, the receiver diameter D_R must also increase.

d. As the number of drones increased, the SNR increased for the proposed system at the suggested parameters.

e. All tests showed that at the SNR < 10dB, there is a trivial betterment in the ABER. After SNR ≥ 10 dB, there are noticeable improvements in system performance.

f. Depending on the measured performance, if the pointing error angle θ_r becomes worst (increase) because of internal or external factors, the GS controller can adjust the link distance Z.

g. The subsystems can be considered as individual and independent parts and used for other different configurations.

h. The selection of suitable receiver diameter D_R depends on the drone's payload and is mentioned in the manufacturer's datasheet.

For pointing error angle θ_r=10^{-3}rad, the link distances Z increased from 10 ~ 50 m per one-centimeter increases of the receiver diameter $D_R \leq 5$ cm. After $D_R > 5$, the link distances Z increased by nearly 100 m per centimeter.

For pointing error angle θ_r=10^{-2} rad, the values of the applicable link distances Z are nearly 10% of the link distances Z values at θ_r=10^{-3}rad. The same percent when increasing the pointing error angle θ_r to 10^{-1}rad.

For pointing error angle $\theta_r \leq 10^{-4}$ rad, the permitted link distance $Z \leq 8500$ m even if the receiver diameter DR is increased to 10 cm.

REFERENCES

[1] P. J. Singh and R. De Silva, "Design and implementation of an experimental UAV network," *International Conference on Information and Communications Technology, ICOIACT 2018,* vol. 2018-Janua, pp. 168–173, 2018, DOI: 10.1109/ICOIACT.2018.8350739.

[2] A. A. Farid and S. Hranilovic, "Outage capacity optimization for free-space optical links with pointing errors," *Journal of Lightwave Technology*, vol. 25, no. 7, pp. 1702–1710, 2007, DOI: 10.1109/JLT.2007.899174.

[3] M. T. Dabiri, S. M. S. Sadough, and M. A. Khalighi, "Channel Modeling and Parameter Optimization for Hovering UAV-Based Free Space Optical Links," *IEEE Journal on Selected Areas in Communications*, vol. 36, no. 9, pp. 2104–2113, 2018, DOI: 10.1109/JSAC.2018.2864416.

[4] W. J. Mazher, H. T. Ibrahim, O. N. Ucan, and O. Bayat, "Drone swarm with free-space optical communication to detect and make deep decisions about physical problems for area surveillance," *Optical. Eng.*, vol. 57, no. 03, p. 1, Mar. 2018, DOI: 10.1117/1.oe.57.3.036116.

[5] T. Song, Q. Wang, M.-W. Wu, T. Ohtsuki, M. Gurusamy, and P.-Y. Kam, "Impact of Pointing Errors on the Error Performance of Intersatellite Laser Communications," *J. Light. Technol.,* vol. 35, no. 14, pp. 3082–3091, Jul. 2017, DOI: 10.1109/JLT.2017.2705132.

[6] N. Ansari, M. Zhou, and T. Zhang, "A Survey on Acquisition , Tracking , and Pointing Mechanisms for Mobile Free-Space Optical Communications," *IEEE Commun. Surv. Tutorials*, vol. 20, no. 2, pp. 1104–1123, 2018, DOI: 10.1109/COMST.2018.2804323.

[7] C. Chlestil, E. Leitgeb, N. Schmitt, S. Muhammad, K. Zettl, and W. Rehm, "Reliable Optical Wireless Links within UAV Swarms," *International Conference on Transparent Optical Networks,* 2006, vol. 4, pp. 39–42, 2006, DOI: 10.1109/ICTON.2006.248491.

[8] Nasa Space Communication, (2018, Nov.). The Optical spectrum. [Online]. Available:https://www.nasa.gov/directorates/heo/scan/engineering/technology/txt_opticalcomm.html

[9] H. Kaushal and G. Kaddoum, “Optical Communication in Space: Challenges and Mitigation Techniques,” *IEEE Commun. Surv. Tutorials*, vol. 19, no. 1, pp. 57–96, 2017, DOI: 10.1109/COMST.2016.2603518.

[10] H. Kaushal, V.K. Jain, and S. Kar, *Free Space Optical Communication*, California, USA, Springer (India), 2.17, pp (5-15), DOI: 10.1016/b978-0-12-813365-1.00008-4.

[11] J. Zhao, F. Gao, Q. Wu, S. Jin, Y. Wu, and W. Jia, “Beam Tracking for UAV Mounted SatCom on-the-Move with Massive Antenna Array,” *IEEE J. Sel. Areas Commun.*, vol. 36, no. 2, pp. 363–375, 2018, DOI: 10.1109/JSAC.2018.2804239.

[12] Z. Ghassemlooy, W. Popoola, and S. Rajbhandari, *Optical wireless communications: System and channel modelling with MATLAB®*. 2017, DOI: 10.1201/b12687.

[13] E. Leitgeb, K. Zettl, S. S. Muhammad, N. Schmitt, and W. Rehm, “Investigation in free space optical communication links between unmanned aerial vehicles (UAVs),” *Proc. 2007 9th Int. Conf. Transparent Opt. Networks, Ict. 2007*, vol. 3, no. 1, pp. 152–155, 2007, DOI: 10.1109/ICTON.2007.4296268.

[14] W. Fawaz, C. Abou-Rjeily, and C. Assi, “UAV-Aided Cooperation for FSO Communication Systems,” *IEEE Commun. Mag.*, vol. 56, no. 1, pp. 70–75, 2018, DOI: 10.1109/MCOM.2017.1700320.

[15] A. A. Khuwaja *et al.*, “A Survey of Channel Modeling for UAV Communications,” *IEEE Commun. Surv. Tutorials*, vol. 20, no. 4, pp. 2804–2821, 2018, DOI: 10.1109/COMST.2018.2856587.

[16] C. Yan, L. Fu, J. Zhang, and J. Wang, “A Comprehensive Survey on UAV Communication Channel Modeling,” *IEEE Access*, vol. 7, pp. 107769–107792, 2019, DOI: 10.1109/ACCESS.2019.2933173.

[17] C. Chlestil *et al.*, “Optical Wireless on Swarm UAVs for High Bit Rate Applications,” in *IEEE CSNDSP*, 2006, no. July 2015, pp. 634–638, 2006, DOI.

[18] S. S. Muhammad *et al.*, “Challenges in establishing free space optical communications between flying vehicles,” *6th International Symposium on Communication Systems, Networks and Digital Signal Processing*, 2008, pp. 82–86, 2008, DOI: 10.1109/CSNDSP.2008.4610721.

[19] E. Bisaillon *et al.*, “Free-space optical link with spatial redundancy for misalignment tolerance,” *IEEE Photonics Technol. Lett.*, vol. 14, no. 2, pp. 242–244, 2002, DOI: 10.1109/68.980535.

[20] A. A. Farid and S. Hranilovic, “Outage capacity optimization for free-space optical links with pointing errors,” *J. Light. Technol.*, vol. 25, no. 7, pp. 1702–1710, 2007, DOI: 10.1109/JLT.2007.899174.

[21] S. Arnon, “Optimization of Urban optical wireless communication systems,” *IEEE Trans. Wirel. Commun.*, vol. 2, no. 4, pp. 626–629, 2003, DOI: 10.1109/TWC.2003.814351.

[22] H. G. Sandalidis, “Optimization models for misalignment fading mitigation in optical wireless links,” *IEEE Commun. Lett.*, vol. 12, no. 5, pp. 395–397, 2008, DOI: 10.1109/LCOMM.2008.071788.

[23] J.-B. Wang, M. Sheng, X. Song, Y. Jiao, and M. Chen, “Comments on `BER Performance of FSO Links over Strong Atmospheric Turbulence Channels with Pointing Errors” *IEEE Commun. Lett.*, vol. 16, no. 1, pp. 22–23, Jan. 2012, DOI: 0.1109/LCOMM.2011.111011.112008.

[24] H. G. Sandalidis, “Coded free-space optical links over strong turbulence and misalignment fading channels,” *IEEE Trans. Commun.*, vol. 59, no. 3, pp. 669–674, 2011, DOI: 0.1109/TCOMM.2011.121410.090318.

[25] H. Zhang and Y. Dong, “Link misalignment for underwater wireless optical communications,” *Proc. - 2015 Adv. Wirel. Opt. Commun. RTUWO 2015*, vol. 16, no. 10,

pp. 215–218, 2015, DOI: 0.1109/RTUWO.2015.7365755.

[26] I. E. Lee, Z. Ghassemlooy, W. P. Ng, and M. Uysal, “Performance analysis of free space optical links over turbulence and misalignment induced fading channels,” *Proc. 2012 8th Int. Symp. Commun. Syst. Networks Digit. Signal Process. CSNDSP 2012*, 2012, DOI: 10.1109/CSNDSP.2012.6292668.

[27] N. a Mohammed, A. S. El-wakeel, and M. H. Aly, “Pointing Error in FSO Link under Different Weather Conditions,” *Int. J. Video Image Process. Netw. Secur.*, vol. 12, no. 1, pp. 6–9, 2012, DOI: .

[28] M. Tawabur Rahman, S. Iqbal, and M. Monjurul Islam, “Modeling and performance analysis of free space optical communication system,” in *2012 International Conference on Informatics, Electronics and Vision, ICIEV 2012*, 2012, no. April 2019, pp. 211–218, 2019, DOI: 10.1109/ICIEV.2012.6317371.

[29] E. Lee, J. Park, D. Han, and G. Yoon, “Performance analysis of the asymmetric dual-hop relay transmission with mixed RF/FSO links,” *IEEE Photonics Technol. Lett.*, vol. 23, no. 21, pp. 1642–1644, 2011, DOI: 10.1109/LPT.2011.2166063.

[30] I. S. Ansari, F. Yilmaz, and M. S. Alouini, “Impact of pointing errors on the performance of mixed RF/FSO dual-hop transmission systems,” *IEEE Wirel. Commun. Lett.*, vol. 2, no. 3, pp. 351–354, 2013, DOI: 10.1109/WCL.2013.042313.130138.

[31] J. Poliak, P. Pezzei, E. Leitgeb, and O. Wilfert, “Analytical expression of FSO link misalignments considering Gaussian beam,” *Proc. 2013 18th Eur. Conf. Netw. Opt. Commun. NOC 2013 2013 8th Conf. Opt. Cabling Infrastructure, OC I 2013*, pp. 99–104, 2013, DOI: 10.1109/NOC-OCI.2013.6582874.

[32] J. Vitasek, E. Leitgeb, T. David, J. Latal, and S. Hejduk, “Misalignment loss of free space optic link,” *Int. Conf. Transparent Opt. Networks*, vol. 2, no. 2, pp. 1–5, 2014, DOI: 10.1109/ICTON.2014.6876494.

[33] M. Sharma, D. Chadha, and V. Chandra, “Performance Analysis of Multihop Free Space

Optical Communication System with Pointing Errors," *J. Opt. Commun.*, vol. 36, no. 1, pp. 24–27, 2015, DOI: 10.1515/joc-2014-0037.

[34] G. Immadi, M. Venkata Narayana, A. Sree Madhuri, and V. L. Tejaswani Sabbasani, "Simulation of free space optical communication under different weather conditions," *Int. J. Pure Appl. Math.*, vol. 117, no. 18 Special Issue, pp. 143–148, 2017, DOI.

[35] S. Singh and G. Soni, "Pointing error evaluation in FSO link," in *IET Conference Publications*, 2013, vol. 2013, no. 645 CP, pp. 365–370, 2013, DOI: 10.1049/cp.2013.2215.

[36] I. E. Lee, Z. Ghassemlooy, W. P. Ng, and M.-A. Khalighi, "Reducing pointing errors in free-space optical communication links over turbulences with a partially coherent Gaussian beam," in *2016 IEEE International Conference on Communications Workshops (ICC)*, 2016, pp. 163–168, 2016, DOI: 10.1109/ICCW.2016.7503782.

[37] A. Harris, J. J. Sluss, H. H. Refai, and P. G. LoPresti, "Alignment and tracking of a free-space optical communications link to a UAV," *AIAA/IEEE Digit. Avion. Syst. Conf. - Proc.*, vol. 1, pp. 1–9, 2005, DOI: 10.1109/DASC.2005.1563300.

[38] S. Sheikh Muhammad *et al.*, "Challenges in establishing free space optical communications between flying vehicles," in *Proceedings of the 6th International Symposium Communication Systems, Networks and Digital Signal Processing, CSNDSP 08*, 2008, pp. 82–86, 2008, DOI: 10.1109/CSNDSP.2008.4610721.

[39] A. Hatziefremidis, K. E. Zarganis, H. C. Leligou, and N. Pleros, "Bit error rate analysis along a slanted path link between UAVs and Ground Stations," in *2013 15th International Conference on Transparent Optical Networks (ICTON)*, 2013, pp. 1–4, 2013, DOI: 10.1109/ICTON.2013.6602799.

[40] A. Kaadan, H. H. Refai, and P. G. Lopresti, "Multielement FSO Transceivers Alignment for Inter-UAV Communications," *J. Light. Technol.*, vol. 32, no. 24, pp. 4785–4795, 2014, DOI: 10.1109/JLT.2014.2364795.

[41] M. T. Dabiri and S. M. S. Sadough, “Optimal Placement of UAV-Assisted Free-Space Optical Communication Systems with DF Relaying,” *IEEE Commun. Lett.*, vol. 24, no. 1, pp. 155–158, Jan. 2020, DOI: 10.1109/LCOMM.2019.2949274.

[42] H. T. Ibrahim and O. N. Ucan, “Drone swarm with free-space optical communication to detect and make deep decisions about physical problems for area surveillance,” vol. 57, no. 3, 2018, DOI: 10.1117/1.oe.57.3.036116.

[43] A. Almarzooqi, I. N. Swamidoss, A. A. S. Al Mansoori, and S. Sayadi, “BER analysis of FSO communication link over UAE weather conditions for UAV applications,” in *Environmental Effects on Light Propagation and Adaptive Systems II*, 2019, no. October, p. 19, 2019, DOI: 10.1117/12.2533048.

[44] A. K. Majumdar, “Free space optical communication,” *LIA Today*, vol. 10, no. 1. Elsevier, p. 1, 2002, DOI: 10.1016/b978-0-12-813365-1.00008-4.

[45] I. I. Smolyaninov, L. Wasiczko, K. Cho, and C. C. Davis, “Long-distance 1.2 Gb/s optical wireless communication link at 1550 nm,” *Free. Laser Commun. Laser Imaging*, vol. 4489, no. June 2014, pp. 241–250, 2002, DOI: 10.1117/12.453237.

[46] A. Gupta, “Comparative Analysis of Free Space Optical Communication System for Various Optical Transmission Windows under Adverse Weather Conditions,” *Procedia - Procedia Comput. Sci.*, vol. 89, pp. 99–106, 2016, DOI: 10.1016/j.procs.2016.06.014.

[47] G. Kaur, H. Singh, and A. Singh Sappal, “Free Space Optical Using Different Modulation Techniques – A Review,” *Int. J. Eng. Trends Technol.*, vol. 43, no. 2, pp. 109–115, 2017, DOI: 10.14445/22315381/ijett-v43p218.

[48] V. Jain and H. Kaushal, “Free Space Optical Communication : Laser sources , Modulation Schemes and Detection,” no. February, 2013.

[49] S. Bloom, E. Korevaar, and J. Schuster, “Understanding the performance of free-space optics [Invited],” vol. 2, no. 6, pp. 178–200, 2003.

[50] SZ DJI Technology Co. Ltd., “Matrice 600". [Online]. Available:

https://www.dji.com/matrice600-pro?site=brandsite&from=eol_matrice600

[51] M. R. Abaza, N. A. Mohammed, and M. H. Aly, “BER performance of M-ary PPM free-space optical communications with channel fading,” in *8th International Conference on High-Capacity Optical Networks and Emerging Technologies, HONET 2011*, 2011, no. December, pp. 111–115, 2011, DOI: 10.1109/HONET.2011.6149799.

[52] A. Prokeš, “Modeling of Atmospheric Turbulence Effect on Terrestrial FSO Link,” *Radio engineering Journal*, vol. 13, no. 3, pp. 42–47, 2009.

[53] S. M. Navidpour, M. Uysal, and M. Kavehrad, “BER performance of free-space optical transmission with spatial diversity,” *IEEE Trans. Wirel. Commun.*, vol. 6, no. 8, pp. 2813–2819, Aug. 2007, DOI: 10.1109/TWC.2007.06109.

[54] C. R. Shah, “Performance and Comparative Analysis of SISO ,SIMO,MISO, MIMO,” *Int. J. Wirel. Commun. Simul.*, vol. 9, no. 1, pp. 1–14, 2017.

[55] M. Abaza, R. Mesleh, A. Mansour, and A. Alfalou, "MIMO Techniques for High Data Rate Free Space Optical Communication System in Log-Normal Channel," *The International Conference on Technological Advances in Electrical, Electronics and Computer Engineering, TAEECE 2013*, pp. 1-5, 2013, DOI: 10.1109/TAEECE.2013.6557185.